

Nanoparticle Synthesis

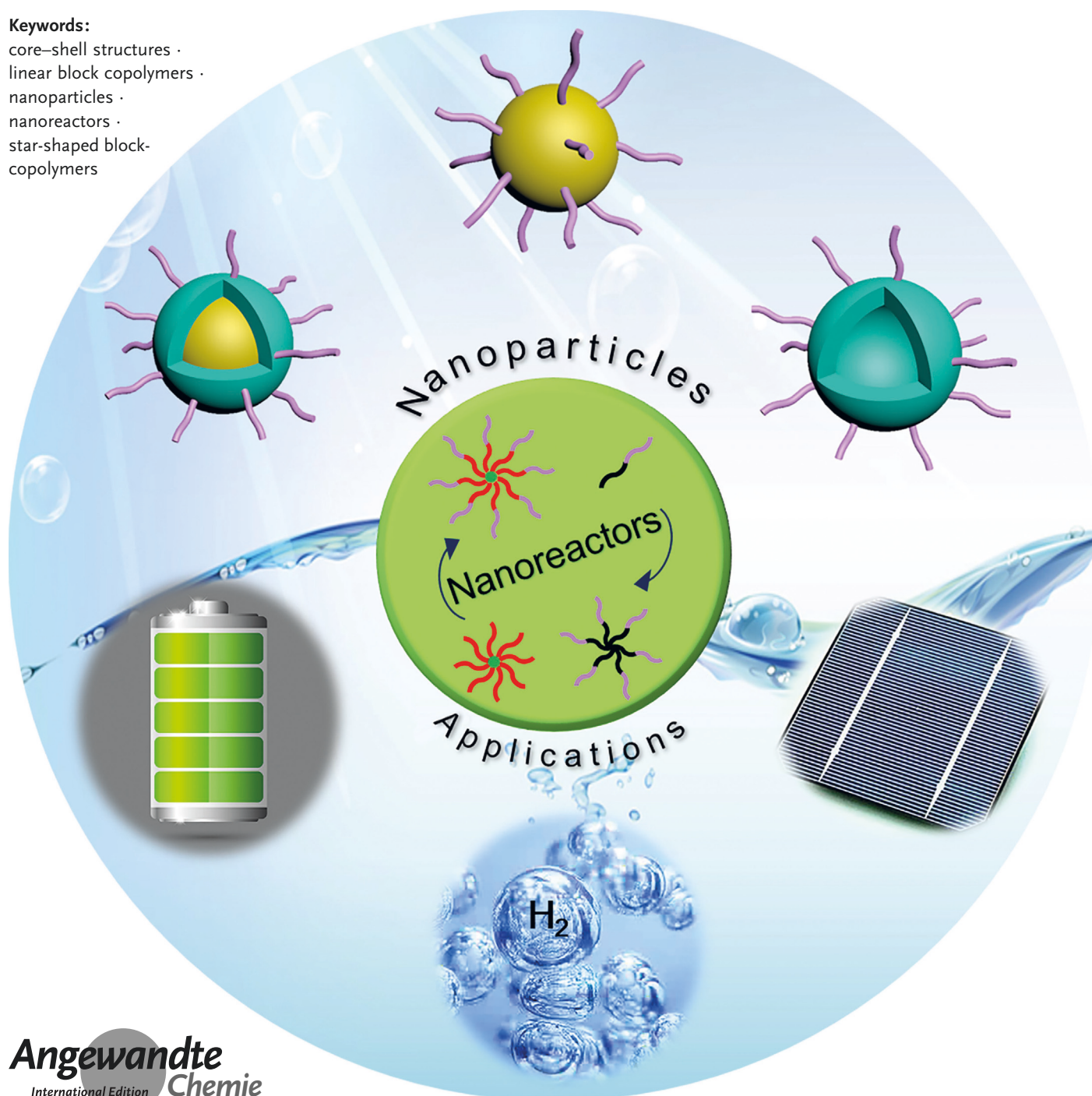
International Edition: DOI: 10.1002/anie.201705019
German Edition: DOI: 10.1002/ange.201705019

From Precision Synthesis of Block Copolymers to Properties and Applications of Nanoparticles

Xiao Li, James Iocozzia, Yihuang Chen, Shiqiang Zhao, Xun Cui, Wei Wang, Haifeng Yu,* Shaoliang Lin,* and Zhiqun Lin*

Keywords:

core-shell structures ·
linear block copolymers ·
nanoparticles ·
nanoreactors ·
star-shaped block-
copolymers



Inorganic nanoparticles have become a research focus in numerous fields because of their unique properties that distinguish them from their bulk counterparts. Controlling the size and shape of nanoparticles is an essential aspect of nanoparticle synthesis. Preparing inorganic nanoparticles by using block copolymer templates is one of the most reliable routes for tuning the size and shape of nanoparticles with a high degree of precision. In this Review, we discuss recent progress in the design of block copolymer templates for crafting spherical inorganic nanoparticles including compact, hollow, and core-shell varieties. The templates are divided into two categories: micelles self-assembled from linear block copolymers and unimolecular star-shaped block copolymers. The precise control over the size and morphology of nanoparticles is highlighted as well as the useful properties and applications of such inorganic nanoparticles.

1. Introduction

Nanomaterials have attracted considerable interest because of their unique physical and chemical properties. Their properties are quite different from their bulk counterparts because of quantum-size effects. In recent years, there has been significant development in the synthesis, functionalization, and application of nanomaterials in many fields, including biology,^[1] optics,^[2] electronics,^[3] and catalysis.^[4a,b] In general, nanoparticles are synthesized by either top-down or bottom-up methods. In top-down methods (i.e. by breaking down), nanoparticles are produced by breaking down bulk materials through the application of strong external forces. This method usually requires extreme conditions, which are typically costly. In addition, it is hard to control the size and shape of the resulting nanoparticles and further functionalize the particles.^[5] For bottom-up methods (i.e. by building up), particles are nucleated and grown. In this way, the size and morphology of the resulting nanoparticles can be tuned by controlling the time and direction of the crystallization process.^[6] Bottom-up strategies such as hydrothermal methods,^[7] organic solution-phase synthesis,^[8] sol-gel processes,^[9] and dendrimer templating^[10] are chemical processes that have been developed to obtain nanoparticles in a simpler and more economical way than top-down methods.^[11]

The two primary issues facing the synthesis and application of nanoparticles are control of the nanoparticle dispersity in solution and control of the size/shape. It is well known that nanoparticles have a strong tendency to aggregate in solution because of the high surface energy and large interfacial area. These properties also complicate the blending of nanoparticles into nanocomposites as well as their self-assembly into sophisticated nanostructures. Chemical treatment after synthesis of the nanoparticles can overcome the problem of their insufficient stabilization in organic solvents or polymer matrices.^[12] Both “grafting-to” and “grafting-from” methods have emerged for passivating nanoparticle surfaces.^[13] Such strategies can effectively prevent nanoparticles from aggregating. However, control over the size and shape remains

a problem, since there is no directed particle formation or methods to limit unwanted growth prior to surface passivation. To this end, the synthesis of nanoparticles with block copolymer nanoreactors has been exploited. Block copolymers can self-assemble thermodynamically into intriguing nanoscale morphologies including spherical, tubular, and worm-like micelles with distinct inner and outer blocks.^[14a-c] The basic concept behind methods based on block copolymer templates is that functional groups in one polymer block provide a directed site for the nucleation and growth of particles, with the other block acting as a capping ligand to prevent the nanoparticles from aggregating.^[15] Block copolymer template methods are favorable since the polymer blocks are tethered to the formed nanoparticles, thus preventing them from aggregating. In addition, the size and shape of the

From the Contents


1. Introduction	2047
2. Synthesis of Inorganic Nanoparticles by Employing Linear Block Copolymer Templates	2048
3. Synthesis of Inorganic Nanoparticles by Using Unimolecular Star-Shaped Block Copolymer Templates	2057
4. Properties of Crafted Nanoparticles	2062
5. Applications of Functional Nanoparticles	2064
6. Summary and Outlook	2067

[*] X. Li, Prof. H. Yu

Department of Material Science and Engineering, and
Key Laboratory of Polymer Chemistry and Physics of the
Ministry of Education, Peking University
Beijing 100871 (P.R. China)
E-mail: yuhaifeng@pku.edu.cn

X. Li, J. Iocozzia, Dr. Y. Chen, Dr. S. Zhao, X. Cui, W. Wang, Prof. Z. Lin
School of Materials Science and Engineering
Georgia Institute of Technology, Atlanta
GA 30332 (USA)
E-mail: zhiquan.lin@mse.gatech.edu

W. Wang, Prof. S. Lin
Shanghai Key Laboratory of Advanced Polymeric Materials
Key Laboratory for Ultrafine Materials of Ministry of Education
School of Materials Science and Engineering
East China University of Science and Technology
Shanghai 200237 (P.R. China)
E-mail: slin@ecust.edu.cn

 The ORCID identification number(s) for the author(s) of this article can be found under:
<https://doi.org/10.1002/anie.201705019>.

nanoparticles can be altered by changing the molecular weight of each block. However, the sizes and shapes of linear block copolymer micelles are only dynamically stable and may deform or completely disassemble as a result of changes in the environment, including solvent composition, concentration, pH value, and temperature.^[16]

Therefore, unimolecular star-shaped block copolymer micelles with structures that are far more stable to environmental factors were introduced as nanoreactors for the synthesis of nanoparticles. Recently, a general and robust strategy for producing nanoparticles within 21-arm unimolecular star-shaped block copolymer nanoreactors was reported.^[11] Not only compact particles, but also hollow and core-shell varieties can be obtained by changing the template structure. The nanoparticles are permanently tethered to polymers, which passivate the surface of the nanoparticles and impart colloidal stability and solubility in a variety of solvents. To date, there have only been a few reviews on the solution-

phase synthesis of inorganic nanoparticles with linear diblock copolymer templates.^[17] Notably, a systematic review of spherical nanoparticles produced by block copolymer templates (especially star-shaped block copolymer templates) has not yet been reported. In this Review, we summarize the synthesis of nanoparticles by using both traditional linear block copolymer templates as well as new unimolecular star-shaped block copolymer templates. The nanoparticles are classified into three main categories depending on their morphology: compact, hollow, and core-shell. The precise control of the size afforded by adjusting the various polymer block lengths and chemical compositions will be the focus of this Review. The properties and applications of such nanoparticles are also summarized.

2. Synthesis of Inorganic Nanoparticles by Employing Linear Block Copolymer Templates

The large surface/volume ratio of nanoparticles can lead to high surface energies and a strong tendency for nanoparticles to aggregate in solution. Stabilizing agents, such as surfactants and polymers, have been applied to the particle surface by ligand exchange or grafted after synthesis of the inorganic nanoparticles to prevent their aggregation.^[18a,b] The connection between a surfactant and a nanoparticle is primarily through weak noncovalent bonding. This connection can be disrupted by high temperature, UV irradiation, and by adjusting the ion concentration and solvent composition.^[19] Ultimately, it is the separation of the polymer



Xiao Li received her BS from the College of Material Science and Engineering at Shandong University. She is currently a PhD candidate at the College of Engineering, Peking University, and has been a visiting PhD student in Prof. Zhiqun Lin's group at Georgia Institute of Technology since 2015. Her research interests focus on the preparation of ordered structures with polymers and nanoparticles by flow-enabled self-assembly methods, as well as the synthesis and applications of photoresponsive liquid-crystalline polymers.



James Iocozzia received his Bachelor of Science in Polymer and Fiber Engineering from the Georgia Institute of Technology in 2012. He is currently pursuing his PhD in the School of Materials Science and Engineering at the Georgia Institute of Technology. His research interests include nanocomposites, block copolymers, and hyperbranched polymer systems for the development of functional nanomaterials in the areas of drug delivery, energy, and stimuli-responsive materials. He is a National Defense Science and Engineering Graduate (NDSEG) Fellow.



Yihuang Chen received his B.E. (2013) and PhD (2017) in Materials Science and Engineering with Prof. Guangzhao Zhang from South China University of Technology. From 2014 to 2017 he was a visiting student in Prof. Zhiqun Lin's group at the Georgia Institute of Technology, where he is currently a Postdoctoral Fellow. His research interests mainly focus on the synthesis of responsive bulk polymers, functional polymer brushes, and polymer/inorganic nanocrystal hybrids for applications in controlled drug release and catalysis.



Shiqiang Zhao received his PhD in Physical Chemistry from Shandong University in 2017. He is currently a postdoctoral research associate in Prof. Zhiqun Lin's group in the School of Materials Science and Engineering at the Georgia Institute of Technology. His research interests focus on the development of advanced electrode materials for lithium ion batteries and lithium sulfur batteries.



Xun Cui received his Bachelor of Engineering in Chemical Engineering and Technology from Jiangnan University in 2012. He is a PhD student at the College of Chemistry and Chemical Engineering at the Chongqing University and currently a visiting PhD student in Prof. Zhiqun Lin's group at the Georgia Institute of Technology. His research interests focus on the development of advanced materials for fuel cells, electrocatalytic and photocatalytic water splitting, and perovskite solar cells.

synthesis stage and the surface passivation stage that typically makes such approaches imprecise. Thus, the synthesis of inorganic nanoparticles within linear block copolymer micelles has been developed as an alternative approach.

This section first introduces the categories of inorganic nanoparticles synthesized using block copolymer templates. Routes for nanoparticle synthesis are then presented together with relevant theory. Lastly, precise control over the formation of compact, hollow, and core-shell nanoparticles is detailed.

2.1. Categories of Inorganic Nanoparticles

Spherical nanoparticles produced using block copolymer micelles as templates can be categorized in three general ways: 1) spherical nanoparticles can be classified by their structure into compact, hollow, and core-shell nanoparticles. 2) They can be grouped by the type of functional material, such as noble metals (Au,^[20] Pd,^[21] Pt),^[22] metal oxides (ZnO,^[23] TiO₂),^[24] metal sulfides (CdS,^[25a-c] ZnS),^[26] and others (Co₂Fe₂O₄,^[27a,b] CaCO₃, BaSO₄). For the synthesis of noble-metal nanoparticles, metal atoms are obtained by either reducing precursors in polymer films with plasma^[15,28a-c] or adding a reducing agent in solution. In this Review, the focus is on the reduction of precursors in solution. 3) The block copolymer template used can also be used to classify the nanoparticles.

As this Review will show, several different types of block copolymer templates have been investigated. Block copoly-

mers are composed of two or more connected polymer blocks that possess specific architectures including linear and star shapes. The simplest example is AB type (where A and B represent two dissimilar polymer blocks), which can be further extended into linear block and star triblock copolymers.^[29] For completeness, we have listed the abbreviation, full name, and chemical structures of the block copolymer templates mentioned in this Review in Table 1. The outermost polymer chains afford the nanoparticles with solubility in either organic or aqueous solution. Nanoparticles soluble in organic solutions are templated from amphiphilic block copolymers with a hydrophilic inner core and hydrophobic outer chains, for example, PS-*b*-P4VP^[20] (template 1a), PS-*b*-P2VP^[30] (template 1b), PS-*b*-PAA^[25a,c] (template 2a), and PS-*b*-PMA^[31] (template 2b). Nanoparticles soluble in aqueous solution are obtained with double hydrophilic block copolymers (DHBCs) such as P2VP-*b*-PEO (template 3),^[32] PEG-*b*-PEI (template 4),^[33a,b] and PAA-*b*-PAM (template 5)^[26] as well as triblock copolymers with a water-soluble corona such as PI-*b*-PCEMA-*b*-PAA (template 6).^[34a,b] Other templates contain functional polymer blocks that provide interesting stimuli-responsive properties including temperature and light. PI-*b*-PCEMA-*b*-PAA with a hydroxylated PI (PHI) corona, a PCEMA cross-linkable intermediate section, and a PAA inner core was used to template γ -Fe₂O₃ and Pd nanoparticles.^[34a,b] The PCEMA shell was first cross-linked to fix the morphology of the micelles. The PI block was then hydroxylated to enable the nanoparticles to be easily dispersed in water. A diblock copolymer template, PDMA-*b*-PNIPAM (template 7), containing a temperature-respon-



Wei Wang received his BS from the School of Chemical Engineering at China University of Petroleum (East China). He is currently a PhD candidate in the School of Materials Science and Engineering at the East China University of Science and Technology under the supervision of Prof. Shaoliang Lin, and has been a visiting student in Prof. Zhiquan Lin's group at the Georgia Institute of Technology since 2016. His research interests mainly focus on the fabrication and manipulation of microstructures by the self-assembly of photosensitive polymers and inorganic nanoparticles.



Shaoliang Lin received his bachelor's degree from the East China University of Science and Technology (ECUST) in 1999 and has been a faculty member there since then. He received his master's degree (2004) and PhD (2007) from ECUST. He was a visiting researcher at the Tokyo Polytechnic University (2005–2006). He became a full professor of ECUST in 2013. His current research interests include macromolecular self-assembly and photosensitive polymers.



Haifeng Yu received his PhD in 2003. After postdoctoral research with Prof. Ikeda at Tokyo, he started his independent scientific career at the Nagaoka University of Technology. Since 2012 he has been a Professor of Materials Science at Peking University. His research focuses primarily on the development of responsive materials based on block copolymers, liquid-crystal polymer composites, and supramolecular polymers. He received a JSPS Fellowship (2005) and was honored by the National Thousand Talents Plan for Young Scholars (2011) and NSFC Outstanding Youth Foundation (2013).



Zhiquan Lin received his PhD in Polymer Science and Engineering from the University of Massachusetts at Amherst in 2002. In 2004 he joined the Department of Materials Science and Engineering at the Iowa State University as an Assistant Professor and was promoted to Associate Professor in 2010. He moved to Georgia Institute of Technology in 2011, and became Professor of Materials Science and Engineering in 2014. His research interests include polymer-based nanocomposites, block copolymers, polymer blends, conjugated polymers, functional nanocrystals, solar cells, batteries, and hydrogen generation.

Table 1: Molecular structure of block copolymer templates.

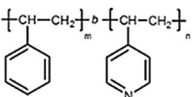
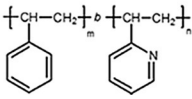
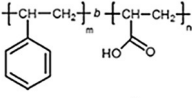
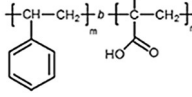
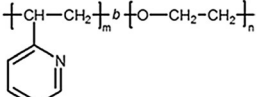
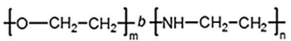
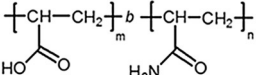
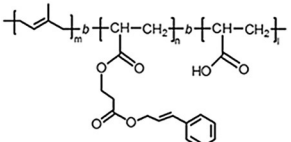
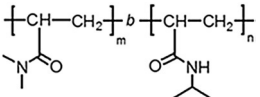
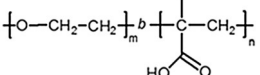
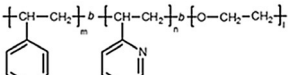
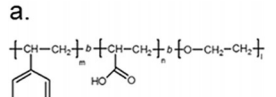
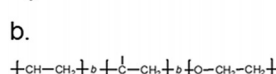
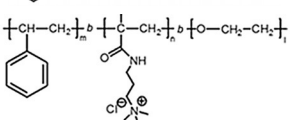
No.	Template ^[a]	Structure	Functional block	Ref.
1	a. PS- <i>b</i> -P4VP / b. PS- <i>b</i> -P2VP polystyrene- <i>b</i> -poly(4-vinylpyridine) / polystyrene- <i>b</i> -poly(2-vinylpyridine)	<p>a. </p> <p>b. </p>	P2VP/P4VP	[20–22, 25b, 30, 52]
2	a. PS- <i>b</i> -PAA / b. PS- <i>b</i> -PMA polystyrene- <i>b</i> -poly(acrylic acid) / polystyrene- <i>b</i> -poly(methylacrylic acid)	<p>a. </p> <p>b. </p>	PAA/PMA	[25a,c, 31, 51a, b]
3	P2VP- <i>b</i> -PEO poly(2-vinylpyridine)- <i>b</i> -poly(ethylene oxide)		P2VP	Ref. [32]
4	PEO- <i>b</i> -PEI poly(ethylene oxide)- <i>b</i> -poly(ethylene imine)		PEI	[33a,b]
5	PAA- <i>b</i> -PAM poly(acrylic acid)- <i>b</i> -poly(acrylamide)		PAA	Ref. [26]
6	PI- <i>b</i> -PCEMA- <i>b</i> -PAA polyisoprene- <i>b</i> -poly(2-cinnamoyl ethyl methacrylate)- <i>b</i> -poly(acrylic acid)		PAA	[34a,b]
7	PDMA- <i>b</i> -PNIPAM poly(dimethylacrylamide)- <i>b</i> -poly(<i>N</i> -isopropylacrylamide)		PDMA	[35]
8	PEO- <i>b</i> -PMAA poly(ethylene oxide)- <i>b</i> -poly(methylacrylic acid)		PMAA	[62a]
9	PS- <i>b</i> -P2VP- <i>b</i> -PEG polystyrene- <i>b</i> -poly((2-vinylpyridine)- <i>b</i> -poly(ethylene glycol))		core: P2VP shell: PEO	[65a–d, 77]
10	a. PS- <i>b</i> -PAA- <i>b</i> -PEG / b. PS- <i>b</i> -PMA- <i>b</i> -PEG polystyrene- <i>b</i> -Poly(acrylic acid)- <i>b</i> -poly(ethylene glycol) / polystyrene- <i>b</i> -poly(methylacrylic acid)- <i>b</i> -poly(ethylene glycol)	<p>a. </p> <p>b. </p>	PAA/PMA	[56, 57, 66a–f, 67]
11	PS- <i>b</i> -PMAPTAC- <i>b</i> -PEO polystyrene- <i>b</i> -poly[(3-(methacryloylamino)propyl)trimethylammonium chloride]- <i>b</i> -poly(ethylene oxide)		PMAPTAC	[68a,b]

Table 1: (Continued)

No.	Template ^[a]	Structure	Functional block	Ref.
12	PMAPTAC- <i>b</i> -PDMAEMA poly[3-(methacryloylamino) propyl trimethylammonium chloride]- <i>b</i> - poly[2-(dimethylamino) ethyl methacrylate]		core: PDMAEMA shell: PMAPTAC	[75]
13	PAA- <i>b</i> -PVDF poly (acrylic acid)- <i>b</i> -poly(vinylidene fluoride)		PAA	[90]
14	PAA- <i>b</i> -PEDO poly (acrylic acid)- <i>b</i> -poly(3,4-ethylenedioxythiophene)		PAA	[91]
15	PLA- <i>b</i> -PDMAEMA- <i>b</i> -PEtOxMA poly(lactide)- <i>b</i> -poly(2-(dimethylamino)ethyl methacrylate)- <i>b</i> - poly[oligo(2-ethyl-2-oxazoline) methacrylate]		PDMAEMA	[100b]

[a] The structure of the functional block copolymers can be employed in linear or star-shaped templates depending on whether they are attached to a multifunctional core.

sive PNIPAM block was also investigated, since the PNIPAM block enables the formation of stable micelles for the formation of inorganic nanoparticles when the solution is heated above the lower critical solution temperature (LCST).^[35]

2.2. Synthesis of Inorganic Nanoparticles by Using Linear Block Copolymer Templates

Block copolymers form self-assembled architectures of defined shapes in specific solvents or solvent mixtures. These self-assembled architectures provide an ideal environment for the controlled, directed growth of nanoparticles. In general, the essential steps of this approach are: 1) polymerization of block copolymers, 2) micellization, 3) precursor loading, and 4) nucleation and growth of nanoparticles.^[17] This general procedure varies for some examples.

2.2.1. Synthesis of Block Copolymers

Block copolymers can be prepared by living anionic polymerization. Most of the linear block copolymer templates in this Review were obtained by this technique. Reversible deactivation radical polymerization (RDRP) has been developed since the early 1990s,^[36] including atom-transfer radical polymerization (ATRP),^[37] reversible addition-fragmentation chain transfer (RAFT),^[38] and nitroxide-mediated free-radical polymerization (NMP).^[39] ATRP and RAFT have widespread application in block copolymer synthesis. Star-shaped block copolymer templates are mainly synthesized through ATRP. Herein, the key aspects of living anionic polymerization, ATRP, and RAFT are introduced.

2.2.1.1. Living Anionic Polymerization

Living polymerization is a form of chain polymerization without chain termination and irreversible chain transfer. The rate of chain initiation is faster than that of chain propagation, which leads to a more constant growth rate of the chain and thus a well-controlled chain length. Living anionic polymerization is a sort of living polymerization which proceeds by an anionic propagation process initiated by the addition of a carbanion complex (e.g. an alkyl lithium compound) as the active species. The advantage of living anionic polymerization lies in the fact that the molecular weight of the polymer can be well-defined because of the absence of chain termination as well as chain transfer without impurities in the system.^[40] The disadvantages of anionic polymerization include the following: the sequence of adding the monomers has to be carefully considered, the types of monomers that can be polymerized are quite limited, and organolithium initiators are particularly dangerous.

2.2.1.2. ATRP

ATRP is a controlled radical polymerization method involving alkyl halides that is catalyzed by transition-metal complexes with organic ligands. The polymerization is a controlled chain-termination process where the organic radical is activated when the halide atom transfers from the alkane halide to the transition-metal complex, and deactivated when the halide atom goes back to the radical on the growing polymer chain.^[36] Thus, the terminal radical on any single growing polymer chain is only active for brief periods of time, thereby allowing only one or two monomer additions prior to being deactivated again. In this way, well-controlled

molecular weights and low polymer dispersity indices (PDIs) can be achieved, as all of the chains essentially grow at the same rate. When using ATRP, consideration of the polymerization sequence for block copolymers is not necessary. However, monomers with reactive groups such as hydroxy, carboxylic acid, and halide groups cannot be directly polymerized using ATRP in the presence of transition-metal complex catalysts.^[41a-c]

2.2.1.3. RAFT Polymerization

In contrast to ATRP, a controlled chain-transfer process is dominant in RAFT polymerization. The transfer reaction is propelled by the addition of an unsaturated chain-transfer agent (RAFT agent) onto propagating radicals. The RAFT agent reversibly couples and decouples from growing polymer chains, thereby reversibly deactivating and activating the radicals and allowing only a few monomers to add during each radical activation. As the chains are mostly deactivated during RAFT polymerization, all of the chains essentially grow at the same rate. Various dithioesters, dithiocarbamates, trithiocarbonates, and xanthates have been successfully used as RAFT agents. RAFT polymerization can be employed for a wide range of monomers, many of which are incompatible with ATRP. Nevertheless, the successful polymerization relies on the appropriate selection or synthesis of RAFT agents.^[42]

2.2.2. Micellization of Block Copolymers

Block copolymers self-assemble into aggregates in specific solvents at a certain temperature above their critical micelle concentration (CMC).^[29] It is interesting that a diverse assortment of micelle morphologies can be realized. The simplest micelles are spherical. Other morphologies include rods, bicontinuous structures, lamellae, tubules, and several others. Eisenberg and co-workers^[14c,43] have summarized the various morphologies that can be obtained in solution and discussed the factors affecting the morphology formed and how to control the morphology of the block copolymer assembly. This Review will focus on the synthesis of spherical nanoparticles. For completeness, some of the theories and terminology related to spherical micelles used throughout this work are first introduced:

Critical micelle concentration (CMC): Below the CMC, block copolymers in solution behave as unassociated unimers (i.e. no self-assembly). Above the CMC, block copolymers self-assemble into micelle structures. The CMC is dependent on several factors, including copolymer type, molecular weight of each polymer block, concentration, temperature, solvent, and pH value.

Aggregation or association number, Z : The number of block copolymers within the micelle. For diblock copolymers, this is generally defined by Equation (1), where N_A and N_B

$$Z \approx N_B^\alpha N_A^{-\beta} \quad (1)$$

are the number of repeat units of insoluble and soluble polymer blocks, and α and β are the scaling exponents of the two blocks, respectively.^[31]

The radius of the micelle core R_c is defined by Equation (2), where κ and γ are the scaling exponents of the two blocks.

$$R_c \approx N_B^\kappa N_A^{-\gamma} \quad (2)$$

The solubility of various micelles in a solvent is closely related to the Flory–Huggins interaction parameter χ . This parameter can be estimated from the Hildebrand solubility parameter δ . For a given system with the block copolymer AB and solvent S, the interaction parameter between a polymer block and the solvent may be given as χ_{AS} [Equation (3)].

$$\chi_{AS} = (\delta_A - \delta_S)^2 v_A / kT \quad (3)$$

Here, δ_A and δ_S are the solubility parameters for the A block and solution, respectively, v_A is the volume of polymer block A, k is the Boltzmann constant, and T is the absolute temperature.

2.2.2.1. Amphiphilic Diblock Copolymers

Amphiphilic diblock copolymers with both hydrophobic and hydrophilic blocks form micelles with a hydrophilic corona in aqueous solution. In organic solvents, they form reverse micelles with hydrophobic outer chains. In organic solvents, the dissolved reverse micelles with a hydrophilic core are favorable for use as nanoreactors, since many inorganic precursors are hydrophilic and/or charged when dissolved. Micellization of amphiphilic block copolymers has been widely researched and summarized in several previous reviews.^[43,44a,b]

2.2.2.2. Double Hydrophilic Block Copolymers (DHBCs)

The introduction of hydrophobicity is typically necessary for the micellization of DHBCs in aqueous solution. Common methods to achieve this goal include complexation with oppositely charged molecules or with hydrophobic molecules. The micellization of DHBCs in aqueous solution is influenced by several factors, including temperature, pH value, and ionic strength, as detailed by Cölfen in a previous review.^[45]

2.2.2.3. Triblock Copolymers

Triblock copolymers are composed of two (ABA) or three (ABC) components. ABA triblock copolymers contain either hydrophilic ends and a hydrophobic middle block, or hydrophobic ends and a hydrophilic middle block. The self-assembly behavior of ABA triblock copolymers in a good solvent for the end blocks is similar to that of diblock copolymers. Micelles with looped or bridged middle chains can form in a poor solvent for the end blocks.^[46]

The micellization of ABC triblock copolymers is more complicated than micellization of diblock copolymers. First, there are six interacting parameters χ_{AB} , χ_{AC} , χ_{BC} , χ_{AS} , χ_{BS} , and χ_{CS} for an ABC triblock copolymer in a certain solvent S, rather than only three, χ_{AB} , χ_{AS} , and χ_{BS} , in the AB diblock copolymer systems. Even for spherical micelles, the ABC triblock copolymer may have different structures. For exam-

ple, PS-*b*-P2VP-*b*-PMMA with two hydrophobic end blocks forms micelles in toluene with a dense P2VP core enclosed by a PS and PMMA corona similar to heteroarm star-shaped copolymers (i.e. miktoarm copolymers).^[47] PS-*b*-P2VP-*b*-PEO can form core-shell-corona (CSC) micelles in water,^[48] which may serve as nanoreactors for hollow or core-shell nanoparticles. In addition to the molecular weight and molecular fraction of each block, the sequence of the three blocks (A-B-C, A-C-B, or B-A-C) also plays a significant role in the morphology of the micelle.^[49a,b]

2.2.3. Precursor Loading

Precursors can be loaded onto the monomer, block copolymer, or polymer micelles. The most common method is to incorporate inorganic precursors into the core of preformed micelles.^[17] The driving force for the incorporation of precursors into micelle cores is based on the electrostatic coordination between the core and various precursors. For example, cations such as Pd²⁺, Co²⁺, and Zn²⁺ can coordinate with pyridine groups present in the micelle core.^[20,33a,50] The reaction rates depend heavily on the precursor type. Precursors with cations (such as from PdCl₂) quickly coordinate directly with the pyridine or PEI blocks. For neutral salts with the metals in an anionic form (such as Na₂PtCl₆, Na₂PtCl₄, and Na₂PdCl₆), the interaction is slower and the precursor loading takes longer. In the case of metals in acidic precursors (such as H₂PtCl₆, HAuCl₄), the acid can protonate the pyridine group to induce an electrostatic interaction that causes fast binding and micellization.^[32] Other polyelectrolytes, such as poly(acrylic acid) (PAA), can interact with precursor ions in a similar fashion.^[25a,c,51a,b]

2.2.4. Nucleation and Growth of Nanoparticles

After loading of the precursors, chemical reactions lead to the nucleation and growth of nanoparticles. For metallic nanoparticles, reducers are introduced to initiate the reaction. For semiconductors, the precipitation of nanocrystals is more common, such as treating a Cd-neutralized PS-*b*-PAA micelle complex with H₂S to precipitate CdS.^[25c] An important parameter for nucleation is the critical nucleation size of a nanoparticle, R_c , which is defined by Equation (4),^[17] where

$$R_c \propto \frac{\gamma}{\ln(c/c_0)} \quad (4)$$

γ is the interfacial tension at the particle/polymer interface and c/c_0 is the degree of supersaturation (the ratio of the precursor concentration to the equilibrium concentration).

2.3. Compact Nanoparticles

This section highlights the precise synthesis of block copolymers. In particular, those factors affecting the size and shape of functional nanoparticles will be addressed. Micelles provide a confined geometry for the growth of nanoparticles. Thus, all the factors that play a role in the micellization of

block copolymers can have an effect on the growth of nanoparticles. Furthermore, nucleation and growth of nanoparticles is also vital for controlling the size of nanoparticles.

2.3.1. Micelle Sizes

The size of the nanoparticles increases with the growth of the micelle core diameter within a certain range. The size of gold nanoparticles templated in PS-*b*-P4VP micelles in toluene was found to correspond directly to the length of the P4VP block.^[20] Larger values of N_{4VP} (P4VP is the insoluble block in this case) in the block copolymer led to an increase in Z and R_c , thus leading to larger Au nanoparticles. However, this effect was limited to a specific range, as observed for CdS nanoparticles.^[25c] For ionic PAA-*b*-PS micelles with core diameters less than 10 nm, the size of the CdS clusters increased linearly with the diameter of the ionic core, with the diameter of CdS ($2R_{CdS}$) increasing from 2.9 nm to 5 nm as the size of the PAA block (N_{AA}) increased from 4 to 32). However, as the core diameter increased beyond 10 nm, the CdS cluster size remained unchanged at 5 nm. The relationship between the size of the nanoparticles and the diameter of the micelle core remains to be established.

2.3.2. Ratio of Precursors to Functional Groups in Block Copolymers

The addition of excess precursors can, to some extent, increase the size of the nanoparticles. Co nanoparticles formed within PS-*b*-P4VP micelles using a Co₂(CO)₈ precursor were investigated at three 4VP/Co²⁺ ratios. Spherical nanoparticles with a size of 10 nm formed at a 4VP/Co²⁺ ratio of 1:1. Star-shaped aggregates with a size of about 20 nm formed at a 4VP/Co²⁺ ratio of 1:2. Lastly, two kinds of particles formed at a 4VP/Co²⁺ ratio of 1:3—cubic particles formed outside the micelles and small spherical particles formed within the cores. Further increasing the Co²⁺ ratio enabled the formation of anisotropic particles, such as rods.^[52] In the Cd²⁺/PS-*b*-P2VP complex micelle system, it was also reported that the UV/Vis absorption band was red-shifted as the 2VP/Cd²⁺ molar ratio was reduced, which indicated larger CdS nanoparticles can be prepared at lower 2VP/Cd²⁺ molar ratios.^[25b]

2.3.3. Types of Reductant

The type of reductant plays a significant role in the formation of nanoparticles. A strong, homogeneous reductant such as NaBH₄ results in raspberry-like Au nanoparticles (simultaneous nucleation at many sites) within one micelle, whereas reduction with hydrazine (N₂H₄) leads to cherry-like Au nanoparticles (single nanoparticle formed per micelle) because of the slower nucleation rate (Figure 1).^[20,53] A similar dependence of the particle shape on the reductant has also been observed for Pd nanoparticles.^[22] The kinetics of the formation of Au nanoparticles with various reducing agents was further studied by Möller and co-workers. Au nanoparticles were prepared with three different reductants: hydrazine (HA), triethylsilane (TES), and potassium tri-

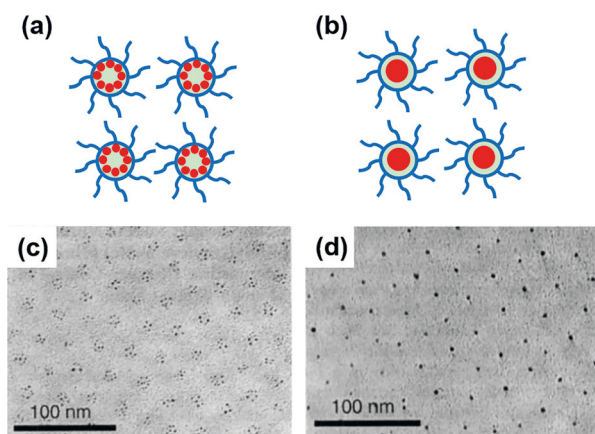


Figure 1. Formation of a) raspberry-like and b) cherry-like metal nanoparticles in block copolymer micelles. Adapted from Ref. [20] with permission, Copyright 1995 Wiley-VCH. TEM images of Au nanoparticles with c) raspberry-like morphology and d) cherry-like morphology. Reprinted from Ref. [53] with permission, Copyright 1996 Wiley-VCH.

ethylborohydride (PTB). After sufficient reduction time, the average diameters of the Au nanoparticles reduced by HA, TES, and PTB were 8 nm, 2.6 nm, and 1.7 nm, respectively. Each reducing agent reacted through a different mechanism. Reduction by TES is an endothermic process. This inhibited the further growth of nanocrystals, thus generating relatively small nanoparticles. Reduction by PTB led to the original micellar structure being rearranged during the course of the reduction, thereby also leading to relatively small nanoparticles.^[54a,b] As previously observed for the reduction of Au by HA, the slower nucleation rate enables the formation of relatively large nanoparticles.

2.3.4. Types of Precursor

The addition of precursors during micellization affects the aggregation number of the micelles that form. Depending on the precursor added during the micellization, the size of the formed micelles can vary and further lead to nanoparticles of various sizes. Block ionomer complex micelles of PS-*b*-PAA containing a wide range of metal ions have been characterized to reveal the scaling relationship between the precursor type and nanoparticle size. The relationship of both Z and R_c with N_A and N_B has already been shown in Equations (1) and (2). In this case, since N_A of the soluble block is a constant, Z and R_c can be expressed by Equations (5) and (6).

$$Z = K_z N_B^\alpha \quad (5)$$

$$R_c = K_R N_B^\kappa \quad (6)$$

In these equations, K_z and K_R are proportionality constants that depend on the metal precursors investigated, N_B is the degree of polymerization of the inner polymer block, and α and κ are the scaling exponents of Z and R_c , respectively. Based on these equations, it was found that Z decreased in the following order: $\text{Ni}^{2+} > \text{Cs}^+ > \text{Co}^{2+} > \text{Ba}^{2+} > \text{Cd}^{2+} > \text{Pb}^{2+}$. This relationship demonstrates the different coordination

capabilities of ions with the inner polymer block, which may be related to the radius of the metal ions. Stronger interactions are expected between the counterions and the charged polymer units as the radius of the divalent cations decreases.^[31]

2.3.5. pH Value in Aqueous Solution

As previously mentioned, the micellization of DHBCs largely depends on the pH value in aqueous solution. PEO-*b*-P2VP forms micelles with a P2VP core when the pH value is larger than 5, and the micelles decompose at lower pH values because of protonation of the pyridine groups.^[32] However, the introduction of metal salts stabilizes the micelles at a pH value as low as 1.8. Changes in the morphology were also observed as the pH value was increased. The incorporation of an acidic HAuCl_4 precursor into spherical PEO-*b*-P4VP micelles led to a retention of the initial geometry, while the incorporation of the neutral gold salt NaAuCl_4 induces a sphere-to-rod transition.^[50]

Block copolymer templating methods offer several advantages over more traditional methods for the synthesis of inorganic nanoparticles. The micelle cores offer sites for nucleation and growth of nanocrystals, and the shell enables the nanoparticles to be well-dispersed in solution. Precise control over nanoparticles is realized in two steps: 1) micellization of the block copolymer, and 2) nucleation and growth of the nanoparticles. All those factors that affect micellization would thus also have an effect on all subsequent steps. The disadvantage of this process is that the self-assembly of linear block copolymers involves only a weak association that can be easily disrupted by changing the external environmental conditions. The susceptibility of templates for hollow and core-shell nanoparticles to environmental conditions is similarly a problem.

2.4. Nanoparticles with Hollow Structures

Hollow inorganic nanoparticles show better performance than conventional solid-core nanoparticles in many applications because of their low density, higher surface-to-volume ratio, low thermal expansion coefficients, and capacity for encapsulating sensitive/reactive materials.^[55] These advantages have prompted their application in several fields including drug delivery,^[56] energy storage,^[57] and wave absorption.^[58] However, hollow nanostructures are much more challenging to make. One strategy for the synthesis of hollow nanoparticles makes use of hard sacrificial templates in which the shape of the template guides the formation of the desired inorganic nanostructure, with the hard templates subsequently removed by dissolution or calcination.^[59a,b] Common templates used in this method include metal crystals, silica nanospheres, and PS latex nanospheres. Although this method has been extensively employed, there are several inherent disadvantages. These include several synthetic steps, which lead to low product yield, and unstable hollow structures after removal of the template. An alternative approach for crafting hollow nanostructures is through

the use of soft templates, including emulsion droplets, surfactant micelles, and block copolymer micelles. For methods based on emulsions and surfactants, the morphology and dispersity of the resulting hollow products are usually poor due to the deformability of soft templates.^[60] Block copolymer micelles can provide a more rigid scaffold for hollow nanostructures, which can lead to better control of the size and shape.^[14c]

2.4.1. Hollow Structures by Utilizing Diblock Copolymer Templates

As previously mentioned, diblock copolymer micelles can serve as nanoreactors for the synthesis of compact nanoparticles when the precursor is loaded into the micelle cores. Similarly, hollow structures can be achieved if the precursors are loaded into the micelle shells. Surface capping ligands are essential for diblock copolymers, otherwise the obtained nanostructures would readily aggregate. Consequently, little work has been done on producing hollow nanostructures with diblock copolymer templates. Hollow zinc borate nanospheres with an outer diameter of 32 nm were synthesized in aqueous solution by using PS-*b*-PAA micelle templates. In this study, the PS core provided the hollow cavity and the PAA corona provided sites for the formation of zinc borate particles.^[61] Submicrometer-sized hollow Ag and CaCO₃ spheres were similarly synthesized by using PEO-*b*-PMAA (template 8) micelles as templates with SDS as a capping ligand.^[62a,b]

2.4.2. Hollow Structures by Using Triblock Copolymer Templates

Triblock copolymer micelles with a core-shell-corona structure can be used to address the absence of surface ligand capping in diblock copolymers.^[63a,b] The intermediate shell block accommodates precursors for the formation of hollow structures, while the corona block serves as a capping layer to improve the solubility and stability of the hollow particles both during and after their formation. Sasidharan and Nakashima have conducted systematic studies on many types of hollow nanoparticles, such as from metal oxides, metal carbonates, metal sulfates, metal borates, and metal phosphates, by using core-shell-corona micelles from ABC triblock copolymers.^[64] Table 2 lists a series of hollow nanospheres produced using different triblock copolymer templates. Each block of an ABC triblock copolymer serves an essential purpose. PEG is used as a corona material so that the hollow particles are soluble in aqueous solution. PS is used as the hollow core (i.e. it prevents coordination of the precursor). For the intermediate shell, functional polymer blocks are employed, including PVP (template 9),^[65a-d] PAA (template 10a),^[56,57,66a-f] PMA (template 10b),^[67] and PMAPTAC (template 11).^[68a,b] Similar to the templated synthesis of compact nanoparticles, the size of hollow structures can be tuned by adjusting several parameters, including the length of each block, the molar ratio of functional groups to precursors, and the pH value.

Table 2: Controlling the size of inorganic hollow nanoparticles templated by linear ABC triblock copolymers.

Template ^[a]	Particle	Size [nm]			Ref.
		Cavity	Shell	Corona	
PS ₁₃₂ -PMA ₁₂₂ -PEG ₄₆	Co ₃ O ₄	30 ± 2	15 ± 1	60 ± 3	[67]
PS ₈₀ -PAA ₉₀ -PEG ₄₇	TiO ₂	16 ± 1	6 ± 1	28 ± 1	[66c]
	CaCO ₃	20	5	30	[56]
	BaSO ₄	16	4.5	25	[66a]
	LaBO ₃	20	7 ± 2	34 ± 2	[66d]
PS ₉₆ -PAA ₁₂₅ -PEG ₄₇	CaP	20	5	30	[57]
	CuO	20 ± 1	10 ± 1	40 ± 1	[66f]
PS ₁₀₇ -PAA ₁₁₆ -PEG ₄₇	ZnO	11	6.9 ± 0.7	24.7 ± 1.3	[66e]
PS ₈₀ -PMAPTAC ₁₀₆ -PEO ₄₇	MoO ₃	16 ± 1	13 ± 1	42 ± 2	[68b]
	WO ₃	14 ± 1	16 ± 1	46 ± 2	

[a] Subscripts denote the degree of polymerization of the various copolymer blocks.

2.4.2.1. Block Length of Triblock Copolymers

It was found that the inner diameter and shell thickness of the resulting hollow inorganic spheres depend on the length of the PS and functional blocks, respectively. As the PS block length increases from 14.1k to 20.1k to 45k, the size of the hollow pore of the obtained nanoparticles increases from 11 nm to 14 nm to 18 nm (Figure 2).^[65c] However, increasing the molecular weight of the PS block further led to solubility problems. This limitation was solved by incorporating linear PS homopolymers (where the molecular weight of the linear homo-PS is similar to that of the PS core in the block copolymer micelles). This enabled additional enlargement of the PS core cavity, which can be tuned from 20.7 nm to 28.5 nm as the weight percentage of linear homo-PS increases from 2 % to 30 % (Table 3).^[65d]

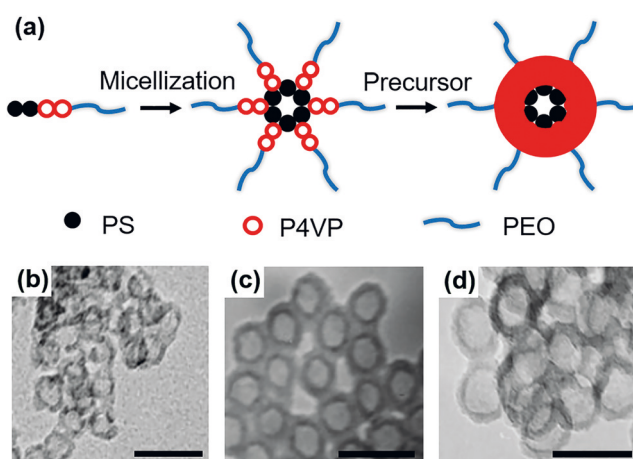


Figure 2. a) Synthetic route to hollow inorganic nanoparticles by using a linear triblock copolymer template. TEM images of hollow silica nanospheres produced using triblock copolymers of different molecular weights: b) PS(14.1k)-PVP(12.3k)-PEO(35k), c) PS(20.1k)-PVP(14.2k)-PEO(26k), d) PS(45k)-PVP(16k)-PEO(8.5k). Scale bar: 50 nm. Reprinted from Ref. [65c] with permission, Copyright 2011 Royal Society of Chemistry.

Table 3: Controlling the size of hollow silica nanoparticles obtained from linear PS-*b*-P2VP-*b*-PEO triblock copolymer templates.

MW of template ^[a]	P2VP/TMOS-molar ratio	Cavity	Size [nm]		Ref.
			Shell	Outer	
14.1k-12.3k-13.5k	1:10	11	6	20	[65a]
	1:15	10.2 ± 0.8	5.9 ± 0.7	22 ± 1.5	
	1:23	11	10	30	
20.1k-14.2k-26k	1:10	14.5 ± 1.4	5.3 ± 0.5	19.8 ± 1.9	[65c]
	1:15	13.9 ± 1.7	5.8 ± 0.4	19.7 ± 2.1	
	1:20	13.8 ± 1.2	7.5 ± 0.7	21.3 ± 1.9	
	1:25	14.0 ± 1.5	7.7 ± 0.8	21.7 ± 2.3	
45k-16k-8.5k	1:15	18.3 ± 1.6	6.4 ± 1.0	24.7 ± 2.6	[65c]
PS-homopolymer (44k) ^[b]					
2%		20.7 ± 1.5	5.0 ± 0.9	30.6 ± 1.7	[65d]
16%		27.0 ± 1.7	5.0 ± 0.8	37.0 ± 1.9	
30%		28.5 ± 2.7	5.1 ± 0.8	38.8 ± 2.9	

[a] Molecular weights of the copolymer template blocks are listed in the order PS-P2VP-PEO. [b] This row shows the influence of added linear PS homopolymer on the size of the hollow nanoparticles formed. Homopolymer-PS (44k) was added into the block copolymer template with a molecular weight of 45k-16k-8.5k at various weight percentages.

2.4.2.2. Molar Ratio of Functional Groups and Precursors

Lower ratios of functional groups to precursors result in the hollow structures having larger diameters. In the case of hollow silica nanospheres obtained from a PS-*b*-P2VP-*b*-PEO triblock copolymer template, the PVP/TMOS molar ratio has a major impact on the shell thickness of the hollow spheres over a particular range (Table 3). Critical ratios for the formation of hollow nanoparticles were observed, with no hollow nanoparticles observed for lower ratios (PVP/TMOS < 1:10), and large aggregates formed at very high ratios (PVP/TMOS > 1:30). At ratios between 1:10 and 1:30, the thickness of the silica shell increased with lower PVP/TMOS ratios.^[65a]

2.4.2.3. pH Value

The effect of the pH value on P2VP-*b*-PEO DHBC micelles has been previously discussed in Section 2.3.5. P2VP becomes hydrophilic after protonation in acidic solution, with decomposition of the micelles at pH < 5. For micelles formed from the PS-*b*-P2VP-*b*-PEO triblock copolymer, the diameter of the PS core remains constant, regardless of the pH value. A reduced pH value did not destroy the micelles, but it did change the thickness of the P2VP shell. It was found that the P2VP block has a size of 5.5 nm at pH > 5 and a size of 8.5 nm at pH < 5. The enlargement of the P2VP shell at pH values less than 5 is due to repulsive forces between the protonated P2VP units.^[48,69] For the synthesis of hollow nanoparticles, the reactions were conducted in an acidic environment. In this way, negatively charged precursors, such as TMOS, can bind strongly to the protonated P2VP block, thereby enabling the formation of a dense silica shell.^[65a] In this case, the acid/base character affords a specific functionality for producing hollow silica nanoparticles.

The use of ABC block triblock copolymers as templates represents a major development in the synthesis of hollow nanoparticles, as it makes possible the production of well-dispersed hollow nanospheres. The size of the hollow spheres can be tuned by adjusting the molecular weight of the templates, the functional polymer/precursor ratio, as well as the pH value. The factors affecting the formation of micelles from ABC triblock copolymers are more complicated than that from amphiphilic diblock copolymers (as discussed in Section 2.2.2), which makes it more difficult to predict the morphology of micelles. In addition, controlling the size of hollow spheres is not as precise as desired. Different nanoparticle sizes can even be obtained with the same templates (PS₈₀-*b*-PAA₉₀-*b*-PEG₄₇; cavity sizes ranging from 16 nm to 20 nm; Table 2). Clearly, obtaining monodisperse hollow particles with precisely controlled sizes and a uniform shape from linear block copolymer templates remains a challenge.

2.5. Nanoparticles with Core-Shell Structures

Generally, core-shell nanoparticles can be classified into two categories: inorganic-organic core-shell nanoparticles and inorganic-inorganic core-shell nanoparticles. In many respects, the compact nanoparticles previously discussed are a sort of inorganic-organic core-shell nanoparticle with a hard inorganic core and an organic polymer corona. The focus in this section is limited to inorganic-inorganic core-shell nanoparticles. In terms of shell materials, core-shell nanoparticles can be divided into silica-coated core-shell nanoparticles and non-silica-coated core-shell nanoparticles.^[70] Encapsulating core nanoparticles with a shell of different materials can provide several advantages: 1) preventing the aggregation of core nanoparticles and enhancing the stability of nanoparticle suspensions in solution;^[71a-c] 2) modulating the position and intensity of the surface plasmon resonance (SPR) band of noble metal nanoparticles;^[72a,b] 3) improving the biocompatibility of nanoparticles.^[73a,b]

Many synthetic techniques have been developed for producing core-shell nanoparticles. The techniques can be summarized into three general approaches.^[74] In the first approach, the shell material is directly nucleated and grown on the surface of the core nanoparticles. This approach is also known as epitaxial growth and requires a small lattice mismatch between the two materials. In the second approach, the shell is grown through chemical reaction of surfactants deposited on the core. This method has been widely used for the synthesis of silica-coated core-shell nanoparticles, since SiO₂ can be easily produced by the hydrolysis of TEOS precursors. In the third approach, both the core precursor and shell precursor are combined in a single-pot reaction. The growth of core nanoparticles was controlled by growth inhibitors, with the shell material subsequently coated on the surface of the nanoparticles. Since the core particles are not purified prior to growth of the shell material, impurities

are easily incorporated between the core and shell components when using this method. This approach is best applied to applications in which lower performance, lower nanocrystal quality, and poorly defined shell thicknesses and coverage are acceptable. However, many end-uses require well-defined core-shell nanostructures. Block copolymers with two functional blocks (typically DHBC and triblock copolymers) can serve as templates for the synthesis of core-shell nanoparticles. In this case, micelles are first prepared, followed by the addition of two different precursors to yield core-shell nanoparticles after reduction. Although there are several reports on this method, systematic studies are limited. Nonetheless, the small amount of work in this area is subsequently reviewed.

2.5.1. Core-shell Nanoparticles by Using Diblock Copolymer Templates

Block copolymer templates provide a better way to control the core size and shell thickness. The double hydrophilic block copolymer PMAPTAC-*b*-PDMAEMA (template 12) was utilized as a template for Ag/SiO₂ nanoparticles. The tertiary amines in the PDMAEMA block coordinate the Ag⁺ ions and supply the electrons for the reduction of Ag⁺ to Ag nanoparticles at the same time. Meanwhile, the PMAPTAC block serves as a reactor for the SiO₂ shell. The core diameter and shell thickness can be controlled by adjusting the molecular weight of each block.^[75] PEO-*b*-PAA also functions as a template for Au-Ag core-shell nanoparticles. The PAA block interacts with a gold precursor, while the neutral PEO block directs the growth of the Ag shell and stabilizes the obtained core-shell nanoparticles.^[76] The uniformity of the particles depends on the Ag⁺ concentration. At low Ag ion concentrations, a uniform shell formed and Au-Ag nanoparticles were obtained. At high Ag ion concentrations, both free Ag nanoparticles and Ag shells grew, which then merged into coupled Au-Ag core-shell nanoparticles.

2.5.2. Core-shell Nanoparticles by Using Triblock Copolymer Templates

Aizawa and Buriak investigated the use of ABC triblock copolymer templates for the synthesis of noble-metal core-shell nanoparticles.^[77] The PS-*b*-P2VP-*b*-PEO triblock copolymer with two functional blocks, P2VP and PEO, was utilized. Anionic gold precursors, such as HAuCl₄, KAuCl₄, and AuCl₃, selectively coordinate with the P2VP block, while the cationic silver precursors favor the PEO block. This template enables the formation of Au@Ag core-shell nanoparticles within the triblock copolymer micelles. Similarly, Sohn and co-workers reported the preparation of Fe@Au core-shell nanoparticles by the coordination of FeCl₃ with P2VP and of LiAuCl₄ with PEO.^[78] Russell and co-workers prepared concentric Pt@Au spheres from PS-*b*-P2VP-*b*-PEO triblock copolymers by sequentially loading H₂PtCl₆ and LiAuCl₄ precursors into the block copolymer micelles.^[79]

Even though the growth of core-shell nanoparticles can be controlled within the block copolymer micelles to some extent, the preparation of core-shell nanostructures from

block copolymer templates remains a complicated process, with only a few reported studies.

3. Synthesis of Inorganic Nanoparticles by Using Unimolecular Star-Shaped Block Copolymer Templates

Star-shaped polymers represent a class of branched macromolecules with linear arms and a central core. They have attracted much attention because of their interesting solution and solid-state properties.^[80] Star-shaped polymers occupy less volume and have lower viscosities than linear polymers of similar molecular weights.^[81] As a consequence of their radial shape, star-shaped polymers are, in a sense, micelles. Conventional micelles are self-assembled from linear block copolymers through weak interactions between the individual molecules, whereas star-shaped polymers are unimolecular micelles where the cores and linear arms are connected through covalent bonding. Thus, star-shaped polymers are more robust architectures that are far less sensitive to environmental perturbations. In this section, the synthesis of star-shaped block copolymers is reviewed, followed by details regarding the templating of inorganic nanoparticles within star-shaped block copolymers. Inorganic nanoparticles synthesized from star-shaped block copolymers include compact, hollow, and core-shell nanoparticles.

3.1. Synthesis of Star-Shaped Polymers and Star-Shaped Block Copolymers

Star-shaped polymers can be prepared by two different approaches: arm-first or core-first methods. In the arm-first methods, the polymer arms are first synthesized and then connected to multifunctional terminating agents or difunctional coupling agents.^[82] In core-first methods, a premade multifunctional core initiates the growth of polymer chains. Compared with the arm-first methods, the core-first approaches afford a higher level of control over the arm numbers through the choice of macroinitiators with a specific number of initiating sites. In the case of polymerizations by ATRP and RAFT, the terminal groups on the polymer arms can continue to be initiated, thus enabling each arm to initiate additional polymerizations to form block copolymers.^[83] The star-shaped block copolymer nanoreactors reviewed herein are obtained by core-first methods that rely on cyclic macroinitiators and controlled/living polymerization.

3.1.1. Multifunctional Initiators for Star-Shaped Block Copolymers

One limitation of core-first methods is the low density of polymer arms resulting from the small number of initiation sites on the small-molecule initiators. Efforts have been made to address this by synthesizing macroinitiators with many initiation sites, including dendrimers,^[84] hyperbranched polymers,^[85] and oligosaccharides (cyclodextrin, sucrose, glucose).^[86]

Cyclodextrins (CD) are cyclic oligosaccharides with six or more repeating glucose units (6, 7, or 8 for α -CD, β -CD, and γ -CD, respectively). CDs have a bowl-shaped structure with a hydrophobic interior and hydrophobic exterior, biocompatibility, and high functionality. These properties make CDs popular in host–guest chemistry and biochemistry. β -CD is composed of 7 glucose units with 7 primary hydroxy and 14 secondary hydroxy groups, thus offering 21 reactive sites. After appropriate chemical modification, β -CD can be employed as a macroinitiator in various polymerization methods. In ATRP, for example, halogenated macroinitiators can be obtained by esterifying the hydroxy groups of β -CD.^[87] Ohno et al. demonstrated that, after modification with 2-bromoisobutryl anhydride, β -CD can be used as a macroinitiator (21-Br- β -CD) for the synthesis of star-shaped polymers.^[88] Li et al. further improved the esterification yield (89.5% compared with 17% in Ohno's work) by esterification with 2-bromoisobutryl bromide.^[89a,b]

3.1.2. Polymerization Techniques for Star-Shaped Block Copolymers

Fast initiation and slow chain propagation is required to obtain star-shaped polymers with comparable arm lengths (i.e. all the arms having similar degrees of polymerization). RDRP and many living polymerizations satisfy these two requirements. However, in a few cases, RDRP is not sufficient to form several important star-shaped block copolymer templates because of polymerization incompatibilities. For this reason, click chemistry has also been employed to graft functional polymer blocks onto preexisting star-shaped polymers and copolymers. Nanoparticles templated by star-shaped block copolymers can be classified by their outer polymer chains as follows: 1) nanoparticles with nonpolar outer polymer chains that can be dissolved in organic solvents, such as PS-capped nanoparticles; 2) nanoparticles with water-soluble polymer chains, such as PEO-capped nanoparticles; and 3) nanoparticles with functional polymer chains, such as PVDF (template 13),^[90] and PEDOT (template 14),^[91] which endow the nanoparticles with added functionalities. In some cases, the functional polymers are produced by polymerization techniques other than RDRP. This section gives an overview of star-shaped polymers synthesized by ATRP, RAFT, and click chemistry from a β -CD macroinitiator.

ATRP is a widely used technique for the synthesis of star-shaped polymers and block copolymers. First, ATRP allows for the well-controlled growth of the polymer chain and low PDIs. Second, the active sites at the end of each polymer chain can be used for further polymerizations or chemical modifications. Several star-shaped polymers, including star-shaped PMCDMA (methyl chloride quaternized poly(2-(dimethylamino)ethyl methacrylate)),^[89a] star-shaped PtBA, and star-shaped PMMA-*b*-PBMA,^[92a,b] have been synthesized by ATRP

with a β -CD initiator. The star-shaped block copolymer templates with PS outer chains described in the following sections are all synthesized by ATRP. Figure 3a shows the synthesis procedure for star-shaped PAA-*b*-PS nanoreactors and templating with inorganic nanocrystals. β -CD is modified into a 21-Br- β -CD macroinitiator, followed by sequential ATRP of PtBA and PS. The PtBA block is then hydrolyzed to form PAA to provide a reactive core for loading the precursors. Since the monomers used in ATRP are quite limited, RAFT can also be used to polymerize certain functional blocks. One example is in the synthesis of star-shaped poly(caprolactone)-*b*-poly(4-chloromethylstyrene) (PCL-*b*-P(S-Cl)). In this case, β -CD was used as a macroinitiator to grow PCL by ring-opening polymerization. Next, a small-molecule RAFT agent was attached to the end of the PCL blocks, thereby forming a RAFT-functionalized star-shaped PCL. Lastly, the 4-chloromethylstyrene monomer was polymerized by RAFT. In this study, the P(S-Cl) block was further modified with azide groups to create photo-cross-linkable star-shaped polymers for the synthesis of soft nanocapsules. However, inorganic nanoreactor templates obtained by RAFT polymerization have not yet been reported.^[93] There are several functional polymers that cannot be grown by either ATRP or RAFT polymerization, thus necessitating their attachment by other means, such as click chemistry.

Click chemistry represents a group of reactions that are modular, widely applicable, proceed in high yields, produce inoffensive by-products, are derived from readily available starting materials, and require only simple product isolation. This concept was first proposed by Sharpless and co-workers, and has been summarized in detail elsewhere.^[94] Click chemistry can be used to graft presynthesized polymer chains onto other polymer chains. Copper-catalyzed azide-alkyne click chemistry (CuAAC) is a common type of click chemistry in which azide (R-N₃) and alkynyl groups react. CuAAC enabled the preparation of 21-arm star-shaped

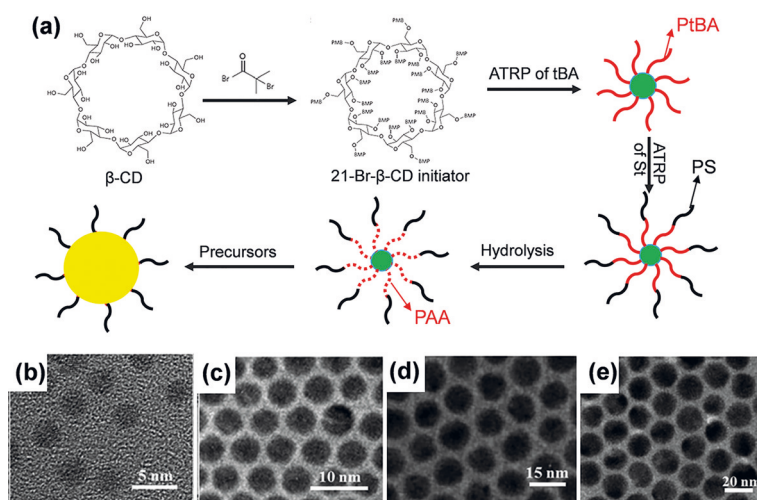


Figure 3. a) Synthetic steps for the preparation of compact nanoparticles by using a star-shaped PAA-*b*-PS diblock copolymer template. b)–e) Au nanoparticles with different diameters: b) 3.2 \pm 0.1 nm (PAA-*b*-PS 3.2k–8.2k), c) 5.1 \pm 0.2 nm (PAA-*b*-PS 4.2k–8.3k), d) 12.2 \pm 0.5 nm (PAA-*b*-PS 11.6k–8.6k), and e) 18.3 \pm 0.4 nm (PAA-*b*-PS 19.1k–6k). Reprinted from Ref. [98] with permission, Copyright 2016 Wiley-VCH.

PNIPAM. β -CD was first brominated to form the macroinitiator 21-Br- β -CD, which was further converted into 21-N₃- β -CD by reaction with sodium azide. Next, alkyne-functionalized PNIPAM was grafted onto the β -CD core.^[95] Star-shaped coil-rod PS-*b*-P3HT (with an inner coil such as PS, and an outer rod such as P3HT)^[96] was obtained by a combination of ATRP and CuAAC. In this approach, PS was first grafted onto 21-Br- β -CD macroinitiator by ATRP. Next, the Br atoms at the end of the PS chains were converted into azides. Lastly, presynthesized alkyne-terminated P3HT was grafted onto the PS chains by CuAAC.^[97] PEO and PVDF are also grafted onto star-shaped polymers in the same way.

The above studies demonstrate the improved stability of unimolecular star-shaped block copolymers compared to micelles from linear block copolymers. Thus, the idea of using unimolecular 21-arm star-shaped block copolymers as nanoreactors for inorganic nanocrystals is a promising approach. The driving force for the synthesis of inorganic nanoparticles is identical to that of linear block copolymer templates, with both relying on coordination between the precursors and functional groups. The following sections give an overview of representative examples of the preparation of inorganic nanoparticles by using unimolecular templates. The specific types addressed include compact, hollow, and core-shell varieties.

3.2. Compact Nanoparticles

The nucleation and growth of nanoparticles within star-shaped block copolymer templates is similar to that in micelles of linear block copolymers (Section 2). The driving force is the coordination between the precursors and the core-forming polymer block. The outer polymer chains permanently tethered to the nanoparticles afford nanoparticles with different properties. The factors affecting the size and shape of the nanoparticles when using star-shaped block copolymer templates are discussed in this section.

3.2.1. Block Copolymer Length

The incorporation of precursors into star-shaped block copolymer templates follows the same approach as employed in micelles of linear block copolymers, as discussed in Section 2.2.3. For star-shaped block copolymer nanoreactors, the length of the inner copolymer block largely dictates the resulting size of the nanoparticles. A rich variety of nanoparticles can be successfully templated by using a typical star-shaped PS-*b*-PAA template. Some of the types produced by this method include Au, Ag, PbTiO₃, BaTiO₃, Fe₃O₄, ZnO, TiO₂, CdSe, Cu₂O, and PbTe. As summarized in Table 4, different kinds of nanoparticles obtained with the same templates show equivalent size. Unlike linear block copolymer templates, in which the precursor loading has an effect on aggregation, the number of micelles, and, therefore, the size of the formed nanoparticles, this complication is not observed for star-shaped systems. That is, a given star-shaped copolymer template yields nanoparticles of the same size from different precursors. This property is reasonable to expect,

Table 4: Compact nanoparticles synthesized from 21-arm β -CD star-shaped diblock copolymer templates.

Template	Template size [nm]	Inorganic nanoparticle size [nm]
PAA- <i>b</i> -PS (4.5k-4.1k)	PAA: 7 \pm 0.5 PAA- <i>b</i> -PS: 22 \pm 0.5	Au: 5.8 \pm 0.2 CdSe: 6.2 \pm 0.3 Cu ₂ O: 6.4 \pm 0.2 Ag: 6.1 \pm 0.3 ZnO: 6.3 \pm 0.3
PAA- <i>b</i> -PS (8.4k-5.2k)	PAA: 11 \pm 0.8 PAA- <i>b</i> -PS: 28 \pm 2.1	PbTiO ₃ : 9.7 \pm 0.4 BaTiO ₃ : 10.4 \pm 0.3 Fe ₃ O ₄ : 10.1 \pm 0.5 TiO ₂ : 10.2 \pm 0.2
PAA- <i>b</i> -PS (6.8k-5.2k)	PAA: 6 \pm 0.2 PAA- <i>b</i> -PS: 39 \pm 1.4	BaTiO ₃ : 6.3 \pm 1.3
PAA- <i>b</i> -PEO (8.4k-5k)	PAA: 11 \pm 0.8 PAA- <i>b</i> -PEO: 28 \pm 2.1	Au: 10.8 \pm 0.5 Pt: 10.2 \pm 0.4 Fe ₃ O ₄ : 10.6 \pm 0.5

since star-shaped block copolymers have a fixed number of arms and core diameter that cannot be affected by the choice of precursors. The templating of a variety of inorganic nanoparticles with star-shaped block polymers has shown that the resulting nanoparticle sizes are highly consistent (Table 4). This makes the star-shaped templates a very general strategy that can be used for a wide range of nanoparticles with predictable size. From this viewpoint, size control is much greater with star-shaped templates than with micelles from linear block copolymers.

By comparing the first and second entries in Table 4, it can be seen that as the PAA block grew from 4.5k to 8.4k, the size of the star-shaped core increased from 7 \pm 0.5 nm to 11 \pm 0.8 nm. Accordingly, the obtained inorganic nanoparticles are between 6–7 nm and 10–11 nm, respectively (as measured by TEM). The diameter of the nanoparticles can be controlled to within \pm 0.5 nm by narrowing the PDI of the block copolymers. The precise control afforded by star-shaped copolymer templates is further demonstrated in Figure 3b–e. A series of PS-capped Au nanoparticles with uniform shape and average diameters from 3 nm to 18 nm were synthesized by using templates with increasing PAA block lengths.^[98] The increasing sizes of the template cores correspond well with the resulting templated Au nanoparticles over the entire range.

3.2.2. Solvents

Although the core diameter in star-shaped templates is the main factor controlling the nanoparticle size, the solvent (or solvents) used in the precursor loading and nanocrystal formation steps also have an impact on the shape of the templated nanoparticles. For example, when templating PbTiO₃ nanoparticles with PAA-*b*-PS, the optimum nanoparticle shape and uniformity is achieved at a DMF/benzyl alcohol (BA) volume ratio of 9:1. Other volume ratios that were investigated included 10:0 and 5:5, but these yielded irregular nanostructures.^[23] The difference stems from the solubility of each polymer block in the solvents. As shown in

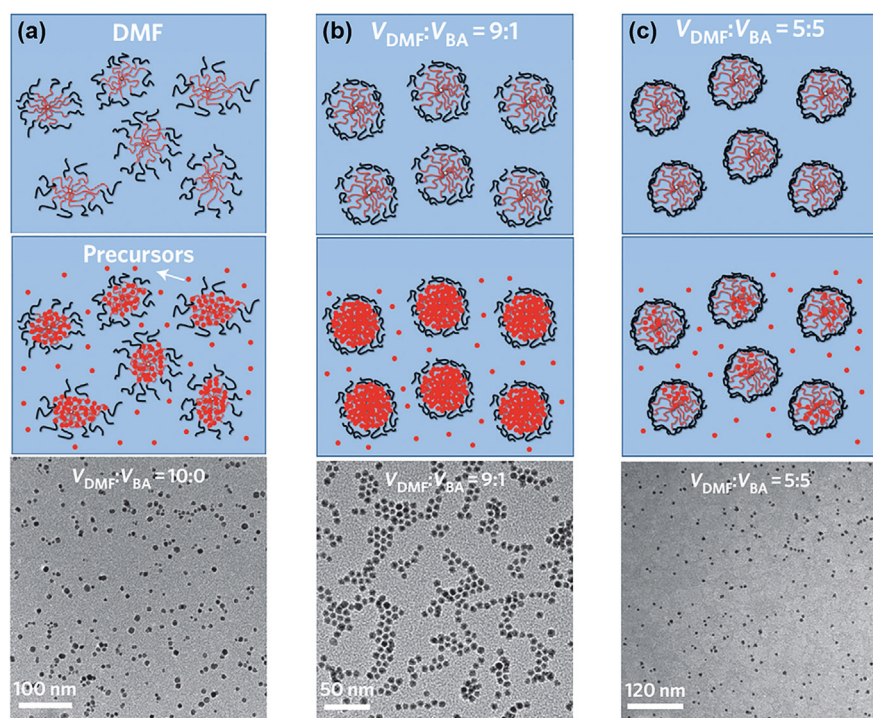


Figure 4. The effect of solvent composition on the shape uniformity of PbTiO_3 nanoparticles synthesized using star-shaped $\text{PS-}b\text{-PAA}$ templates. a) $\text{DMF/BA} = 10:0$ (pure DMF); b) $\text{DMF/BA} = 9:1$; c) $\text{DMF/BA} = 5:5$. The top panels illustrate the formation of the unimolecular micelles in solution. The central panels depict the micelles during precursor loading. The bottom panels are TEM images of the obtained nanoparticles synthesized under the three different solvent compositions. Reprinted from Ref. [11] with permission, Copyright 2013 Nature Publishing Group.

Figure 4, star-shaped $\text{PAA-}b\text{-PS}$ can be readily dissolved in pure DMF as a unimolecular micelle with both extended PAA and PS copolymer blocks (Figure 4a). BA is a good solvent for PAA and a poor solvent for PS, thus the PS blocks collapse onto the PAA core on addition of a small amount of BA ($\text{DMF/BA} = 9:1$), while the PAA retains its coil-like conformation (Figure 4b). This mixed solvent produces more compact and structurally stable spherical structures for improved templating of inorganic nanoparticles. Further increasing the amount of BA ($\text{DMF/BA} = 5:5$) results in the PS shell collapsing to form a more condensed layer on the PAA core. This hinders reaction between the precursors and the PAA block (Figure 4c). The optimum solvent and ratio can vary for the two different precursor systems according to the chemistry of the outer polymer block. For example, when templating BaTiO_3 nanoparticles with $\text{PAA-}b\text{-PVDF}$, the ideal DMF/BA ratio is 5:5.^[90] In contrast, the ideal DMF/DPE (diphenyl ether) volume ratio is 9:1 for $\text{Fe}_3\text{O}_4/\text{Au}$ core-shell nanoparticles templated with $\text{P4VP-}b\text{-PAA-}b\text{-PEO}$.^[99]

3.2.3. Molar Ratio of Reactive Polymer Precursors

Similar to micelle templates from linear block copolymers, the size of the templated nanoparticles can also be affected by the molar ratio of the reactive polymers to precursors. The $[\beta\text{-CD-(PLA-}b\text{-PDMAEMA-}b\text{-PEtOxMA)}_{21}]$ (template 15) star-shaped template has been

reported to be a unimolecular nanoreactor for the synthesis of gold nanoparticles in aqueous solution.^[100a,b] Within the template, the intermediate PDMAEMA block serves as both a stabilizer and a reducing agent to convert the coordinated AuCl_4^- precursors into gold nanoparticles. As the PDMAEMA/ HAuCl_4 ratio was decreased (i.e. less functional polymer block and/or more precursor) from 16 to 6 to 3, the corresponding size of the Au nanoparticles increased from 2.1 nm to 15.8 nm to 21.4 nm, respectively. The stability of the unimolecular micelles decreases as the amount of HAuCl_4 precursor in solution increases. This leads to the coalescence of Au nanoparticles and to larger Au nanoparticle aggregates.

3.2.4. Necklace-like Structured Nanoparticles

Complex, hierarchical structures such as 1D necklace-like nanostructures composed of inorganic nanoparticles have also been prepared by using a templating method based on an $\alpha\text{-CD}$ -based rotaxane. The “shish kebab”-like nanostructures are composed of a stretched PEG polymer chain with threaded inorganic nanodiscs along its length. It has been reported that $\alpha\text{-CD}$ formed high yields of the crystal complex with PEG.^[101] This threaded rotaxane template relies on the propensity for $\alpha\text{-CD}$ to periodically assemble along the PEG chain. The $\alpha\text{-CD}$ units are locked onto the PEG chain by affixing

bulky end groups to the ends. After sequential ATRP of PtBA and PS with the threaded $\alpha\text{-CD}$ -based macroinitiator, the PtBA blocks are hydrolyzed to PAA to yield the final necklace-like template. Inorganic nanodiscs composed of CdSe and BaTiO_3 can be grown by taking advantage of the coordination between metal precursors and the carboxylic acid groups on the PAA chains. The resulting threaded inorganic nanodisc structures can be several hundred nanometers in length.^[102] The above strategies for making various compact nanoparticles can also be generalized to hollow systems.

When compared with linear block copolymer micelles (Section 2), there are fewer external factors that influence the size and shape of the nanoparticles when templating with star-shaped templates. This is to be expected, since star-shaped block copolymer templates are more rigid and possess a fixed arm number and core size. In contrast, linear block copolymer templates are flexible and have a highly variable core size and shape as the aggregation number changes.

3.3. Nanoparticles with Hollow Structures

As mentioned in Section 2.4, noble-metal nanoparticles with hollow interiors are a popular research topic because they have a wide range of applications in controlled drug release, bioimaging, photothermal therapy, and environmen-

tal remediation.^[103] For example, hollow Au nanoparticles have important optical applications related to their absorbance of NIR light, plasmonic resonance,^[104] and surface-enhanced Raman spectroscopy (SERS).^[105] The surface plasmon resonance (SPR) frequency of hollow Au structures is sensitive to the diameter of the inner cavity and the shell thickness.^[106] Star-shaped block copolymer templates provide an excellent approach for obtaining hollow nanostructures with precisely tunable cavity size, shell thickness, and outer polymer corona thickness.

Hollow nanoparticles have been crafted by capitalizing on micelles of linear block copolymers as templates, as shown in Figure 2, Table 2, and Table 3. However, these hollow structures have poorly defined shapes and large variations in their size. Compared with linear triblock copolymers, the arms of star-shaped triblock copolymer PS-*b*-PAA-*b*-PS templates are connected to the β -CD core through a strong covalent bond, which shows a larger tolerance to the surrounding environment (Figure 5a).^[96,97] By using this strategy, added precursors directly react with the middle PAA block without the need for sacrificial templates. Cu₂O (PS-capped) and water-soluble hollow Au nanoparticles (PEO-capped) have been synthesized from hollow Au that is soluble in organic solvents (Figure 5b,c). The inner diameter and wall thickness of the structures can be adjusted by altering the length of the inner PS chains and intermediate PAA chains, respectively (Table 5).

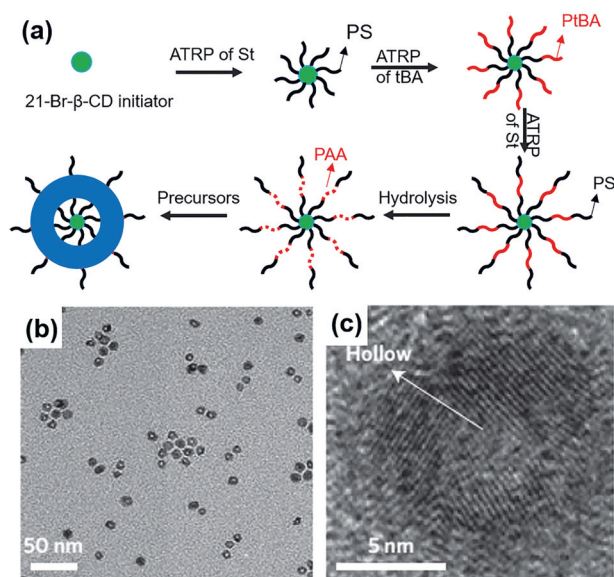


Figure 5. a) Synthesis of hollow nanoparticles templated with a star-shaped PS-*b*-PAA-*b*-PS triblock copolymer template. b) TEM and c) HRTEM images of hollow Au nanoparticles. Reprinted from Ref. [11] with permission, Copyright 2013 Nature Publishing Group.

Table 5: Core-shell and hollow nanoparticles synthesized from β -CD-based 21-arm star-shaped triblock copolymer templates.

Template for core-shell nanoparticles ^[a]	Template size [nm]	Nanoparticle size [nm]
P4VP- <i>b</i> -PtBA- <i>b</i> -PS (6.6k-8.5k-6k)	P4VP: 5.8 ± 0.2 P4VP- <i>b</i> -PtBA: 11.5 ± 0.4	Fe ₃ O ₄ /Au: $6.1 \pm 0.3/2.9 \pm 0.2$ Fe ₃ O ₄ /PbTiO ₃ : $6.1 \pm 0.3/3.1 \pm 0.3$
P4VP- <i>b</i> -PtBA- <i>b</i> -PEO (3k-15k-5k)	P4VP: 11.2 ± 0.5 P4VP- <i>b</i> -PtBA: 22.9 ± 1.1	Sn/Pt: $10.4 \pm 0.1/2.8 \pm 0.4$ Fe ₃ O ₄ /Au: $10.8 \pm 0.5/3.1 \pm 0.3$
Template for hollow nanoparticles	Template size [nm]	Nanoparticle size [nm]
PS- <i>b</i> -PAA- <i>b</i> -PS (4.5k-4.8k-5.6k)	PS: 6.9 ± 0.3 PS- <i>b</i> -PAA: 13.4 ± 0.6	hollow core: 5.6 ± 0.4 Au shell: 3.2 ± 0.3
PS- <i>b</i> -PAA- <i>b</i> -PS (10.1k-9.5k-1.6k)	PS: 10.7 ± 0.7 PS- <i>b</i> -PAA: 25.2 ± 1.4	

[a] The molecular weights of each copolymer block are listed in parentheses below each copolymer abbreviation in the template column.

3.4. Nanoparticles with Core-Shell Structures

Heterogeneous, composite, and sandwiched colloidal semiconductor nanoparticles frequently have enhanced properties compared to single-component systems. In some cases they even develop new properties. This is the motivation behind synthesizing core-shell nanoparticles. However, there are some drawbacks in the aforementioned methods for synthesizing core-shell nanoparticles: 1) aggregation of core nanoparticles during the reaction; 2) shell materials form individual nanoparticles instead of coating the core; 3) impurities collect between the core and shell layers, thereby leading to incomplete coverage of the cores;^[70] 4) the two crystals must have similar lattice parameters (usually less than 10% difference) to form a high-quality core-shell interface.^[107] Consequently, inorganic-inorganic core-shell nanoparticles with uniform shapes and low dispersities are rarely reported.

The synthesis of core-shell nanoparticle templates is essentially an extension of the synthesis of hollow nanoparticle templates, as shown in Figure 6a. The template is a triblock copolymer with two functional blocks: PAA and P4VP. The core and shell precursors react sequentially with the two polymers. With the two precursors reacting independently and no interfacial lattice requirement, core and shell materials with a significant lattice mismatch can even be realized. For example, the lattice parameters of Au and Fe₃O₄ are 0.40786 nm (JCPDS No.26-1136) and 0.8090 nm (JCPDS No.26-1136), respectively. As a consequence of the large lattice mismatch, it is a great challenge to prepare high-quality Fe₃O₄@Au core-shell nanoparticles.^[108] Figure 6b-d shows several core-shell nanoparticles obtained from star-shaped block copolymer templates. It was observed that shell materials perfectly cover the core materials, while maintaining a well-defined round shape.

The core size and shell thickness can be adjusted to desired values by varying the chain length of the core and shell polymer blocks in the templates (Table 5). A series of Fe₃O₄@Au core-shell nanoparticles^[99] (6 nm fixed Fe₃O₄ core with a varied Au shell thickness of 5 nm, 10 nm, and 18 nm; and 5 nm fixed Au shell with varied Fe₃O₄ cores of 6 nm, 10 nm, and 20 nm) as well as Au@TiO₂^[109] nanoparticles

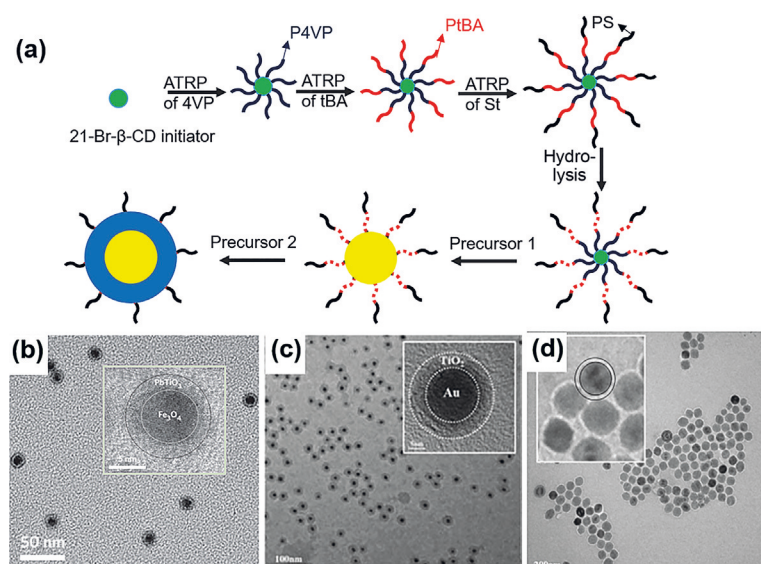


Figure 6. a) Synthetic route to core-shell nanoparticles templated with a star-shaped PS-*b*-PAA-*b*-PS triblock copolymer template. b) TEM and HRTEM images of Fe₃O₄@PbTiO₃ core-shell nanoparticles. a,b) Adapted from Ref. [11] with permission, Copyright 2013 Nature Publishing Group. c) TEM and HRTEM images of Au@TiO₂ core-shell nanoparticles. Reprinted from Ref. [131] with permission, Copyright 2015 American Chemical Society. d) TEM and HRTEM images of Fe₃O₄@Au nanoparticles. Reprinted from Ref. [99] with permission, Copyright 2015 Wiley-VCH.

(15 nm Au core with 1 nm, 5 nm, and 10 nm TiO₂ shell thicknesses; and 5 nm fixed TiO₂ shells with 5 nm, 10 nm, or 15 nm Au cores) have been prepared. These results demonstrate the highly tunable nature of the core-shell nanoparticles produced using this unimolecular star-shaped block copolymer nanoreactor approach.

Star-shaped block copolymer templates with fixed arm numbers and controllable molecular weights for each block form unimolecular micelles with high stability in solution. This provides a robust and general method for the synthesis of nanoparticles. In particular, star-shaped templates display several advantages over linear block copolymer micelles in crafting hollow and core-shell nanostructures. The high quality nanoparticles obtained with star-shaped block copolymer templates offer a good opportunity for understanding structure-property relationships in materials for various applications. It is worth noting that star-shaped unimolecular micelles may suffer from secondary aggregation. The aggregation behavior depends sensitively on the solution concentration and the solvent. The four-arm star-shaped PPO-*b*-PEO with a hydrophilic outer chain and a hydrophobic inner core was found to undergo aggregation in aqueous solution when the concentration was higher than $1 \times 10^4 \text{ mg L}^{-1}$. Both the number and degree of aggregation increase as the concentration increases.^[110] The aggregation issue can be alleviated by tuning the solvent and lowering the polymer concentration.

4. Properties of Crafted Nanoparticles

There are several robust block copolymer templating strategies for synthesizing inorganic nanoparticles. However,

research into the properties and applications of inorganic nanoparticles produced with block copolymer templates is limited. In the following sections, the properties and applications of these inorganic nanoparticles templated by block copolymers are outlined.

4.1. Size-Dependent Properties of Functional Nanoparticles

The properties of functional nanoparticles are highly dependent on their size. This is largely a consequence of the ratio of surface atoms to interior atoms. It is amazing when one considers that a small metal nanocrystal with a diameter of 1 nm has 100 % of its atoms on the surface, while a nanocrystal with a diameter of 10 nm has only 15 % of its atoms on the surface.^[111] The distribution of surface and volume atoms can cause different electronic properties, thereby leading to divergent properties as the particle sizes are reduced. As a consequence of the improved control over their size and shape, the star-shaped block copolymer template methods summarized above offer convenient ways to investigate size-dependent properties. In this section, the surface plasmonic properties and magnetic properties of nanoparticles prepared with star-shaped block copolymer templates are discussed.

4.1.1. Surface Plasmon Resonance (SPR)

4.1.1.1. Compact Nanoparticles

SPR is an optical phenomenon resulting from the interaction between an electromagnetic wave and the conduction electrons in metal nanostructures.^[112] When the frequency of the incident photons matches that of the surface electrons of a metal nanostructure, resonance occurs and the photons will be absorbed by the metal nanostructures. The resonant photon wavelength is dependent on the metal.^[113] Au nanoparticles are the most intensively researched plasmonic nanoparticles with well-understood SPR properties: 1) the characteristic UV absorbance is around $\lambda = 520 \text{ nm}$; 2) as the core size decreases, the maximum intensity decreases, accompanied by a broadening of the band width and a slight blue-shift;^[114] 3) for Au NPs between 1.1 and 2.0 nm in size, the SPR property disappears and step-like spectral structures appear.^[115a,b] Figure 7a,b illustrates the SPR properties of Au and Ag nanoparticles of various sizes. All the nanoparticles were obtained using star-shaped PAA-*b*-PS block copolymer templates. As the size of the Au and Ag nanoparticles increases, the characteristic SPR band increases and the full-width-at-half-maximum (FWHM) narrows. This corresponds well with the literature and indicates the formation of well-defined plasmonic nanoparticles obtained using star-shaped block copolymer templates.^[98]

4.1.1.2. Core-Shell Nanoparticles

Unlike compact nanoparticles, core-shell nanoparticles display more interesting and complex SPR properties, as both constituents can contribute to the observed absorption. In several examples, Au has been used as either the shell

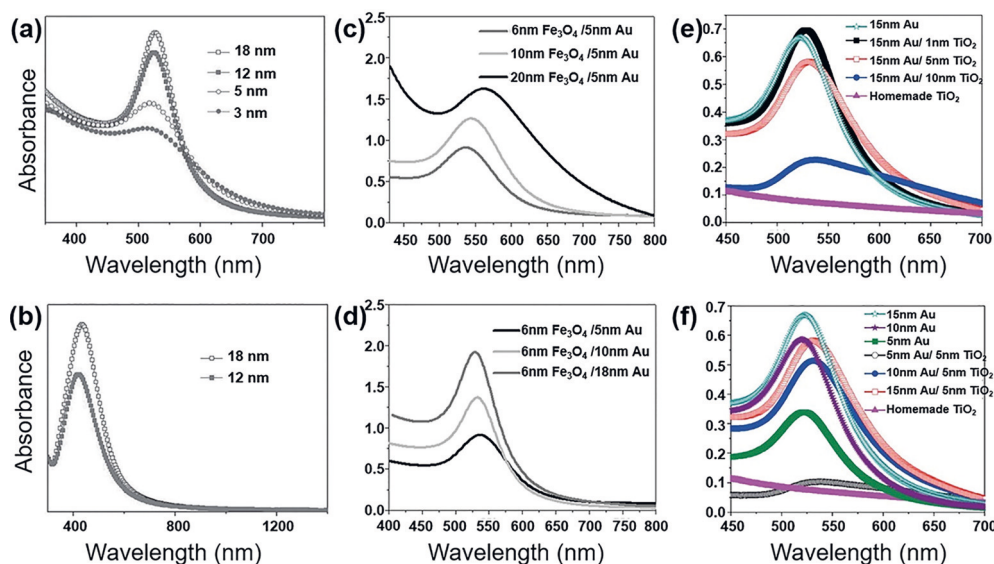


Figure 7. Surface plasmon resonance (SPR) properties of nanoparticles of various sizes. a) Pure Au nanoparticles and b) pure Ag nanoparticles. The SPR intensity goes up as the particle size increases, and the full-width-at-half-maximum (FWHM) narrows accordingly. a,b) Reprinted from Ref. [98] with permission, Copyright 2016 Wiley-VCH. c) Fe_3O_4 @Au core-shell nanoparticles with fixed Au shell thicknesses and varied core diameters. The SPR bands for 6, 10, and 20 nm Fe_3O_4 cores lie at 530, 540, and 563 nm, respectively. d) Fe_3O_4 @Au core-shell nanoparticles with fixed Fe_3O_4 core diameters and varied Au shell thicknesses. The SPR bands for 5, 10, and 18 nm Au shells lie at 537, 533, and 528 nm, respectively. c,d) Reprinted from Ref. [99] with permission, Copyright 2015 Wiley-VCH. e) Au@ TiO_2 core-shell nanoparticles with a fixed Au core diameter and varied TiO_2 shell thicknesses. f) Au@ TiO_2 core-shell nanoparticles with a fixed TiO_2 shell thickness and varied Au core diameters. e,f) Reprinted from Ref. [109] with permission, Copyright 2016 Royal Society of Chemistry.

material (Figure 7c,d) or as the core material (Figure 7e,f). For Fe_3O_4 @Au core-shell nanoparticles with a fixed thickness of the Au shell, increasing the Fe_3O_4 core diameter results in red-shifted SPR bands (Figure 7c).^[99] This phenomenon is consistent with earlier reports for Fe_3O_4 @Au core-shell nanoparticles synthesized by other means.^[116] Both electron population variation theory and plasmon mode coupling theory have been adopted to explain this phenomenon. For Fe_3O_4 @Au core-shell nanoparticles with a fixed core diameter and various Au shell thicknesses, the absorption band shifts to shorter wavelengths (Figure 7d) as the Au shell thickness increases. As the Au shell becomes thicker, the ratio of Au to Fe_3O_4 increases, which leads to a blue-shift of the SPR peak towards the characteristic band of pure Au NPs ($\lambda = 520$ nm). When Au is used as a fixed-size core material, the SPR band of nanoparticles with thicker TiO_2 shells is red-shifted due to the increase in the refractive index of the local dielectric environment around the Au core by coating with a TiO_2 shell (Figure 7e).^[117] The change in the SPR is similar to that of pure Au nanoparticles when the Au core is varied but the TiO_2 shell thickness is fixed (Figure 7f).

4.1.2. Superparamagnetic Properties

The magnetic behavior can be defined by two parameters: residual magnetization (M_r , the magnetization without an applied external magnetic field) and saturated magnetization (M_s , the maximum magnetization with increasing magnetic

field strength). Superparamagnetic nanoparticles have a fast response to externally applied magnetic fields without any residual magnetization ($M_r = 0$).^[118] Superparamagnetism occurs when the size of magnetic nanostructures (such as Fe_3O_4) decreases to a critical radius r_c , where a single domain is formed instead of multiple domains, as in bulk materials. The M_s value of superparamagnetic nanoparticles is also size-dependent. For example, a series of Fe_3O_4 nanoparticles with various sizes (6 nm, 10 nm, and 16 nm) were prepared using star-shaped PAA-*b*-PS templates. The magnetization of these nanoparticles showed no hysteresis loop, which indicates the presence of superparamagnetism. As the particle size increases, the M_s value increases accordingly.^[119]

4.2. Nanocomposites Containing Inorganic Nanoparticles

Incorporating nanoparticles within a polymer matrix often confers advantageous optical, electrical, magnetic, dielectric, and mechanical properties to the resulting composites in proportion to the loading content. The simplest method for obtaining nanocomposites is by physically mixing nanoparticles into a polymer matrix. The simplicity of this approach is countered by the inherent incompatibility of inorganic nanoparticles and a polymer matrix (large interaction parameter $\chi_{\text{NP-Polymer}}$ between the nanoparticle and polymer matrix), which makes it challenging to obtain well-dispersed nanoparticles. The use of a block copolymer template approach results in the surface of the nanoparticles being covered with a polymer layer, which can provide improved miscibility and dispersion of the nanoparticles within the polymer matrices.^[120] With improved dispersion in the polymer matrices, it becomes possible to create functional nanocomposites in areas such as ferroelectrics, magnetics, and thermoelectrics.

4.2.1. Dielectric and Ferroelectric Nanocomposites

Ferroelectricity exists in materials with a spontaneous electric polarization that can be reversed by an external field. Barium titanate (BaTiO_3) is a representative ferroelectric material with a high dielectric constant.^[121] The ferroelec-

tricity of BaTiO₃ nanoparticles depends heavily on the temperature and nanoparticle size. BaTiO₃ nanoparticles possess a tetragonal ferroelectric phase below the Curie temperature ($T_c \approx 130^\circ\text{C}$) and exhibit ferroelectric properties. Above the T_c value, BaTiO₃ nanoparticles convert into a cubic structure with paraelectric properties. Nanosized BaTiO₃ has a lower dielectric constant and depressed ferroelectricity as the particle size decreases. Ferroelectricity disappears when the size decreases to a critical value (dependent on the synthetic method).^[122]

The dielectric properties of block copolymer/ferroelectric nanocomposites were explored by mixing PS-capped BaTiO₃ nanoparticles together with PS-*b*-PMMA block copolymers. The PS chains covalently attached to the particle surface hinder aggregation of the BaTiO₃ nanoparticles and enable their exclusive accumulation within the PS domain of the PS-*b*-PMMA block copolymer. The nanocomposites exhibit high dielectric constants and the dielectric constant decreases as the BaTiO₃ nanoparticle size decreases.^[123]

The polymer matrix itself can have additional functionalities besides encapsulation of nanoparticles. One such functional polymer matrix is poly(vinylidene fluoride) (PVDF). PVDF was attached to the surface of star-shaped nanoreactors by the click reaction, thereby resulting in BaTiO₃ nanoparticle/PVDF nanocomposites. Tuning the molecular weight of the functional block of the templates can change both the size of the nanoparticles as well as the ratio of the nanoparticles to PVDF. Compared with pure PVDF, the nanocomposites exhibited higher dielectric constants, enhanced breakdown strength, and lower dissipation factors (Figure 8a,b).^[40] The improved performance is attributed to the large interfacial area in the nanocomposites. The ferroelectricity of the nanocomposites was further verified by piezoresponse force microscopy (PFM) (Figure 8b,c). The square-shaped hysteresis loop in Figure 8c (phase loop) is consistent with a 180° switching of the permanent polarization, while the butterfly-shaped loop in Figure 8d (amplitude loop) exhibits well-defined spontaneous polarization even in nanoparticles as small as 10 nm.

4.2.2. Thermoelectric Nanocomposites

Thermoelectric materials can directly convert temperature differences into electric voltage and vice versa. They provide an alternative way to generate electricity, and have recently attracted much attention. Thermal conductivity (κ) and electrical conductivity (δ) are both important parameters for a thermoelectric material. Lead telluride (PbTe) is an important TE material which is also semiconducting. Nanocomposites of PbTe nanoparticles dispersed in conductive polymers have been investigated to improve the electrical conductivity of PbTe. The interface between the nanoparticles and polymer play an essential role in preparing nanocomposites with good performance. By using star-shaped block

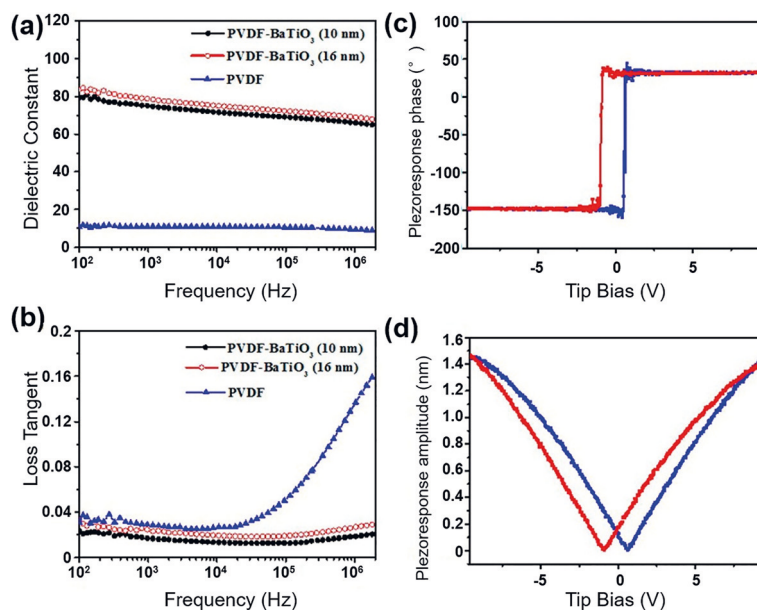


Figure 8. a) Dielectric constant and b) loss tangent (dissipation factor) of pure PVDF polymer and PVDF-BaTiO₃ nanocomposites with BaTiO₃ nanoparticles of different diameters. The nanocomposites exhibit higher dielectric constants and lower dissipation factors (especially in the high frequency range) compared to pure PVDF. c,d) Piezoresponse of a single PVDF-functionalized BaTiO₃ nanoparticle ($D = 10.2 \pm 0.6$ nm) on a TEM grid: c) phase and d) amplitude of the first harmonic signal as a function of V_{dc} to the tip, while a 2 V peak-to-peak ac voltage is applied to the bottom electrode. Reprinted from Ref. [90] with permission, Copyright 2015 American Chemical Society.

copolymer templates, PbTe nanoparticles covalently capped with conducting PEDOT polymer chains were prepared and well-dispersed in a PEDOT polymer matrix. The strong connection between the PbTe nanoparticles and PEDOT polymer chains promotes transport of charge carriers (electrons and holes) and reduces interfacial scattering.^[91] The next section details some of the most relevant areas where well-defined nanostructured materials can have the most impact.

5. Applications of Functional Nanoparticles

The most attractive characteristic of nanoparticles prepared with block copolymer templates is their high stability. In addition, the outer polymer chains can enhance their performance in various applications. To date, nanoparticles generated with block copolymer templates have been applied in several fields including catalysis, solar cells, and lithium ionic batteries (LIBs). In this section, the applications of functional nanoparticles templated by block copolymers are discussed.

5.1. Catalysis

Functional nanoparticles have been applied in catalysis because of their enhanced surface areas compared to bulk materials.^[124a,b] A common problem is that nanoparticles tend to aggregate into larger clusters with small molecular ligands.

This leads to a reduction in the active surface area which lowers the catalytic performance.^[125] It is for this reason that noble metal nanoparticles stabilized with block copolymers have been applied as catalysts.

5.1.1. Compact Nanoparticles in Catalysis

Pd colloids templated within PS-*b*-P4VP micelles were first used as a catalyst in Heck coupling reactions. In these studies, several traditional catalysts in addition to PS-*b*-P4VP-stabilized Pd nanoparticles were applied for the coupling of 4-bromoacetophenone and styrene. The yields from the reaction using each catalyst were compared. Several Pd catalysts stabilized with small-molecule ligands tend to form Pd black, an aggregation of Pd colloids, which leads to moderate product yields (30–35%), whereas templated Pd nanoparticles display much higher catalytic performance (73–92% for different concentrations), and excellent stability (remaining dispersible for several months). It was also found that the catalytic efficiencies of Pd nanoparticles were significantly affected by the size of the nanoparticles and the length of the outer polymer chains. The smallest nanoparticles exhibited the best catalytic activity because of their enhanced surface areas. In contrast, Pd nanoparticles with longer outer polymer chains showed lower activity, since longer polymer chains lead to steric hindrance which reduces the contact between the Pd nanoparticles and reactants.^[21]

Interestingly, the catalytic performance of Pd nanoparticles prepared from water-soluble block copolymer templates can be tuned by adjusting the pH value, thereby enabling a simple and atypical method of catalytic control. Pd nanoparticles prepared using PHI-*b*-PCEMA-*b*-PAA core-shell-corona micelles (the outer PI block was hydroxylated to form water-soluble PHI) were employed to catalyze hydrogenation reactions. In the case of vinylacetic acid (VAA), the rate of hydrogenation was relatively low at pH 10 and gradually increased up to pH 3. This is attributed to the repulsion between the deprotonated PAA blocks and deprotonated VAA substrate at basic pH values.^[34b]

Water-soluble Au (also Pd and Pt) nanoparticles with an average diameter of 10 nm synthesized from linear PEO-*b*-PAA DHBC templates were used as a reducing agent for the decomposition of nitroarenes. The catalytic performance was assessed by the turnover frequency (TOF), which represents the degree of reaction per unit time per amount of catalyst used in the reaction. It was noted that the DHBC-templated Au nanoparticles (800 h⁻¹) displayed a higher TOF than that of Au nanoparticles prepared by reduction with citrate (570 h⁻¹). The surrounding polymer chains likely play an important role in enhancing the catalytic performance by keeping the particles from aggregating over time at both elevated temperature and extreme pH values.^[126] Similar observations were also reported for dendrimer-templated nanoparticle catalysts.^[127a,b] The enhanced performance was attributed to the steric confinement effect of the dendrimer templates on the nanoparticles. Similarly, polymer-stabilized Pd and Au/Pd bimetallic nanoparticles were used as hydrogenation catalysts.^[22] In each case, higher stability and selectivity were observed with polymer-capped catalysts.

The role of the outer polymer chains in the enhancement of the catalytic reactivity still requires further investigation.

5.1.2. Core-shell Nanoparticles in Catalysis

Coating a shell layer onto nanoparticles is another way to avoid activity-reducing aggregation. In addition, favorable properties can be derived from the interaction between compatible core and shell materials.^[128] For example, early research suggests that metal nanoparticles deposited on TiO₂ nanostructures undergo equilibration of the Fermi level following excitation with UV light and possess enhanced efficiency in charge-transfer processes.^[129] Au@TiO₂ core-shell nanoparticles with well-controlled core diameters and shell thicknesses were obtained by using a star-shaped P4VP-*b*-PAA-*b*-PEO template and these were employed in photocatalysis. The photocatalytic rate was evaluated by degradation of rhodamine B (RhB). The reaction rate is expressed by Equation (7).

$$\ln (C_t/C_0) = |k|t, \quad (7)$$

Here, C_t is the concentration of RhB at time t , C_0 is the initial RhB concentration, $|k|$ is the first-order reaction constant, and t is time. The performance of three nanoparticle catalysts—block copolymer templated Au@TiO₂ core-shell nanoparticles, block copolymer templated TiO₂ nanoparticles, and commercial TiO₂ (P25)—were compared. The block copolymer templated TiO₂ nanoparticle catalysts had a similar activity to P25. The Au@TiO₂ core-shell catalysts exhibited much higher activity (Figure 9).^[109] This is attributed to two factors. First, the enhanced light harvesting by the SPR-active Au core enabled greater energy uptake. Second, the Schottky junction formed at the interface between the conductive Au core and semiconducting TiO₂ shell led to enhanced transfer of photo-generated electrons and holes from the Au core to the TiO₂ shell. Of the core-shell structures with fixed TiO₂ shells (5 nm), Au@TiO₂ with a 10 nm Au core showed the highest reaction rate (Figure 9b). This is likely because the smaller Au cores (5 nm) show a relatively weak SPR and the larger Au cores (15 nm) have less surface contact with the TiO₂ shell.

5.2. Solar Cells

5.2.1. Compact Nanoparticles

The polymer chains on the outside of the nanoparticles can play an important role in solar cell applications. NaYF₄:Yb/Er upconversion nanoparticles (UCNPs) prepared using star-shaped PAA-*b*-PEO templates have been used in solar cells. Specifically, PEO-capped UCNPs were employed as mesoporous electrodes with tunable pore sizes (the pore size can be tuned by adding PEO homopolymer) in organolead halide perovskite solar cells (Figure 10a).^[130] The performance of devices with an UCNP layer is better than devices with a conventional TiO₂ layer under near infrared (NIR) irradiation at $\lambda = 918$ nm (Figure 10b). It is likely that, in conjunction with the growth and crystallization of perovskite facilitated by the NaYF₄:Yb/Er UCNPs, the upcon-

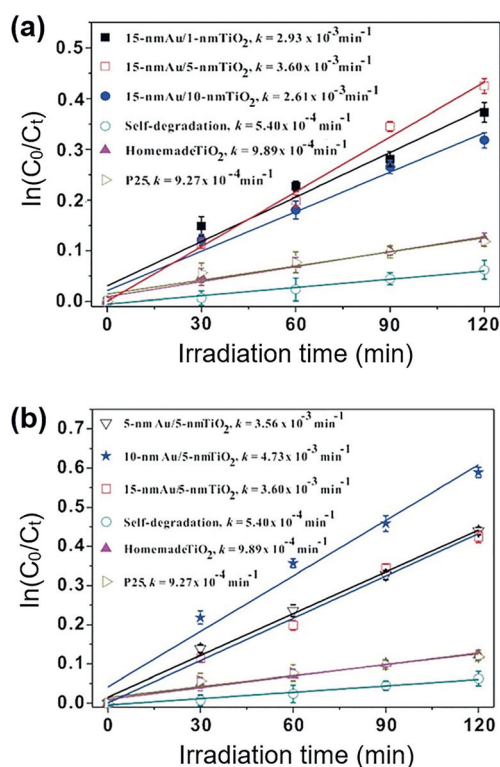


Figure 9. Catalytic performance of Au@TiO₂ core-shell nanoparticles with varied core diameters and shell thicknesses. a) Fixed Au core diameter (15 nm) and varied TiO₂ shell thicknesses. b) Fixed TiO₂ thickness (5 nm) and varied Au core diameters. Reprinted from Ref. [109] with permission, Copyright 2016 Royal Society of Chemistry.

version effect of NaYF₄:Yb/Er UCNPs enhanced the light harvesting and improved the device efficiency. It is worth noting that the outer PEO chains impart not only good solubility and long-term stability to the nanoparticles but also facilitate the formation of the mesoporous structure. The pore sizes of the mesoporous structures can be tuned by adding PEO homopolymer (Figure 10c). Mesoporous structures with larger pores were advantageous for the penetration of perovskite into these structures (Figure 10d). This penetration promotes absorption of the incident photons and transport of charge carriers throughout the electrodes.

5.2.2. Core-shell Nanoparticles

PS-capped Au@TiO₂ core-shell nanoparticles combined with widely used TiO₂ network films were utilized as photoanodes in dye-sensitized solar cells (DSSCs). The PS layer on the Au@TiO₂ nanoparticles was removed by calcination in air or carbonized in an inert atmosphere to

afford uncoated Au@TiO₂ nanoparticles and C-Au@TiO₂ nanoparticles. Both of them exhibited improved performance in DSSCs compared to devices with commercial P25 films. The addition of uncoated Au@TiO₂ core-shell nanoparticles improves the short-circuit current density (J_{sc}) by 10 % and the PCE by 7.4 %. This is explained by two factors: 1) the light harvesting efficiency is improved by the SPR effect of Au cores and 2) sintering of the TiO₂ shell at high temperature resulted in it converting from an amorphous into an anatase phase. C-Au@TiO₂ nanoparticles enabled an even greater enhancement in the performance (increase in J_{sc} by 18.4 % and a PCE increase of 13.6 % compared to commercial P25 TiO₂ films). The performance enhancement is attributed to the conductive carbon layer increasing the electron collection efficiency by reducing the electron-transfer time and extending the lifetime of the electrons.^[131]

5.3. Lithium Ion Batteries

5.3.1. Compact Nanoparticles

On their own, compact nanoparticles do not offer especially attractive performances in lithium ion batteries (LIBs). The addition of an outer carbon layer can improve their electrochemical performance. It is for this reason that block copolymer-templated nanoparticles are employed in LIB applications. ZnFe₂O₄ nanoparticles crafted using PS@PAA nanospheres were implemented in LIB applica-

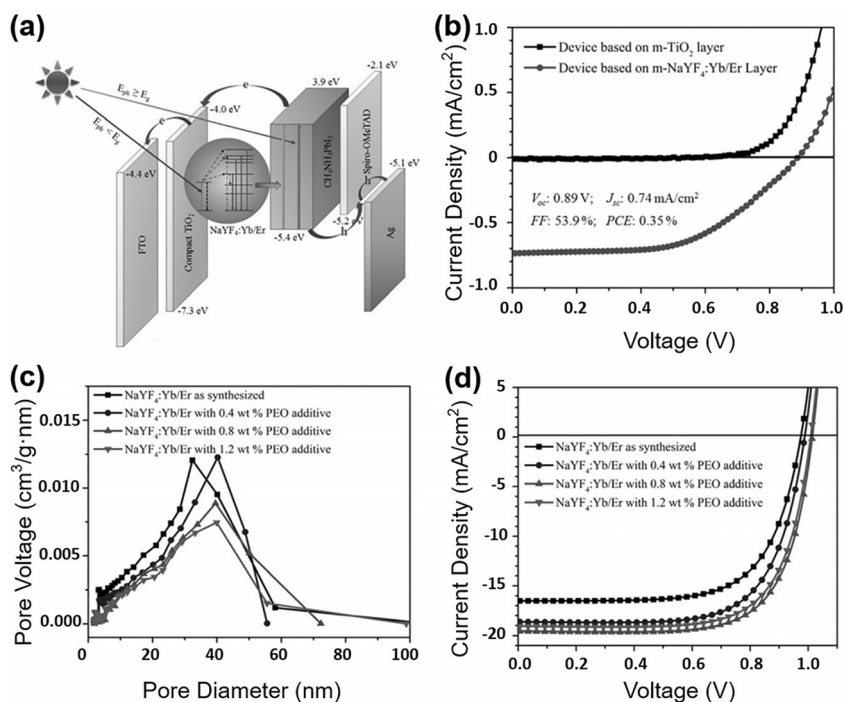


Figure 10. a) Energy levels and charge-transfer processes in perovskite solar cells with NaYF₄:Yb/Er UCNPs as the mesoporous electrode. b) The current density-voltage (J - V) characteristics of perovskite solar cells using a NaYF₄:Yb/Er UCNPs layer and a TiO₂ layer under irradiation with NIR light at $\lambda = 980 \text{ nm}$. c) Change in the pore diameter of the mesoporous structure with different amounts of added linear PEO. d) Current density of perovskite solar cells with varied PEO additives. Reprinted from Ref. [130] with permission, Copyright 2016 Wiley-VCH.

tions. PS@PAA nanospheres not only serve as reactors for the growth of ZnFe_2O_4 nanoparticles, but also provide a latent carbon source in terms of the outer PS layer after thermal decomposition in an inert atmosphere.^[132] Figure 11 a–c shows TEM images of carbonized and uncoated ZnFe_2O_4 nanoparticles. The ZnFe_2O_4 /carbon nanocomposites exhibit the best performance (79.3 wt % carbon). After 70 cycles at a current density of 100 mA g^{-1} , an ultrahigh capacity of 1500 mAh g^{-1} was observed. This is approximately three times the capacity of uncoated ZnFe_2O_4 nanoparticles (Figure 11 d,e). The carbon coating stabilizes the structure and improves the conductivity of the inner nanoparticles. In addition, the continuous carbon network maintained the integrity of the ZnFe_2O_4 nanostructures during cycling.

5.3.2. Hollow Nanoparticles

The well-defined morphologies and sizes of hollow nanostructures play a critical role in enhancing the cycling and rate performance of lithium ion battery (LIB) electrodes. There are two advantages afforded by hollow structures from block copolymer templates: 1) Hollow architectures can provide a larger contact area with the electrolyte and effectively accommodate the volume changes that occur during lithiation–delithiation processes. The volume change during charging and discharging is the single biggest hurdle limiting the improvement of battery lifetime and storage capacity. 2) The small grain size of the hollow spheres shortens the diffusion path during cycling and creates more active sites for charge-transfer reactions. This effectively shortens the lithium ion transport distance and improves the structural stability of the active materials.^[133] Hollow silica nanospheres templated from triblock copolymer micelles (both PS-*b*-PMAPTAC-*b*-PEO and PS-*b*-P2VP-*b*-PEO) enable high cycling perfor-

mance through an alloying/dealloying process.^[65c,134] After 100 cycles at a charging rate of 1 C, the capacity retention of the hollow silica nanospheres (93.4 %) was much higher than that of bulk Si powder (70.7 %). By using the same synthesis method, TiO_2 ,^[66c] CuO ,^[66f] and Co_3O_4 ^[67] were also employed as anode materials for lithium batteries.

6. Summary and Outlook

In this Review, we first summarized the methods for the synthesis of spherical inorganic nanoparticles (compact, hollow, and core–shell) by using linear block copolymers and star-shaped block copolymers as templates. Strategies for tailoring the block copolymer templates to control the size and shape of the inorganic nanoparticles were highlighted. The nanoparticles obtained in block copolymer nanoreactors are permanently tethered to polymer chains through covalent bonding. This confers several advantages over the traditional noncovalent anchoring of small-molecule ligands to nanoparticle surfaces: 1) the outer polymer chains suppress aggregation of the nanoparticles and enhance the solubility of the nanoparticles in various organic solvents; 2) polymer ligands improve the compatibility and dispersion of nanoparticles in various polymer matrices; 3) the size and shape of the nanoparticles can be controlled by adjusting the different copolymer blocks in the templates.

Star-shaped block copolymers have several advantages as templates over linear block copolymers. First, unimolecular micelles are insensitive to external perturbations to the environment such as solvent, pH value, and temperature, thus making the synthesis of inorganic nanoparticles easier to perform and easier to control. The defined spherical shapes of unimolecular star-shaped block copolymers ensure the formation of uniformly shaped nanoparticles during templating. Second, unimolecular star-shaped block copolymer templates afford better control over size and shape. The nanoparticle size is mainly determined by the molecular weight of the functional blocks. In contrast, in the case of linear block copolymers, the particle size corresponds to the micelle size, which in turn is related to the molecular weight of each block in the linear block copolymer, the environmental conditions, and the precursor type. As a consequence, templating with linear block copolymer micelles is a far more challenging technique to use because of the abundance of variables and interrelated properties that affect it.

The improved size control afforded by star-shaped block copolymer templates has enabled a series of investigations into their specific size-dependent properties. The size-dependent properties reviewed include the SPR absorbance of Au nanoparticles and magnetic properties of

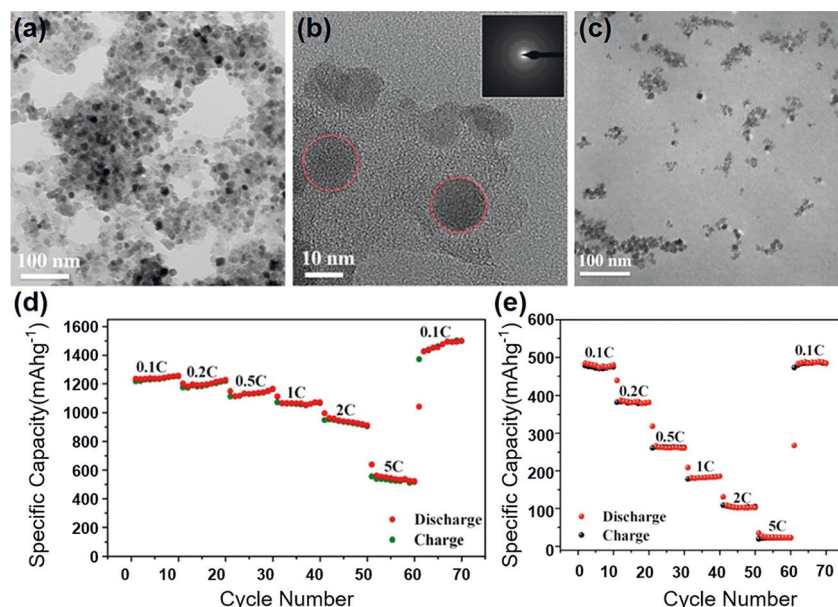


Figure 11. a) TEM and b) HRTEM images of ZnFe_2O_4 /carbon nanocomposites. c) TEM image of uncoated ZnFe_2O_4 nanoparticles. d) Rate performance of ZnFe_2O_4 /carbon nanocomposites and e) ZnFe_2O_4 nanoparticles. Reprinted from Ref. [132] with permission, Copyright 2016 American Chemical Society.

Fe₃O₄. Nanocomposites with advanced dielectric and ferroelectric properties for applications such as catalysis, solar cells, and lithium ion batteries were also detailed, with each property benefiting greatly from the well-defined nanocomposite structures.

Unimolecular star-shaped block copolymer templating methods have provided an attractive way to produce nanoparticles with well-defined sizes and morphologies. Although the synthetic routes have been actively studied, the properties and applications of polymer-capped nanoparticles are still limited in scope. This is especially the case for hollow nanoparticles and core-shell systems. More attention should be given to property- and application-driven research of various nanoparticles combined with functional polymers. For example, the SPR properties of hollow Au spheres, the magnetic properties of Fe₃O₄ nanoparticles, and the applications of emerging functional materials such as perovskite, thermoelectric, and ferroelectric nanoparticles.

The morphology of nanoparticles produced using block copolymer templates is not only limited to spherical shapes. Templating can also be extended to anisotropic rod-like and Janus structures. As previously discussed, Janus star-shaped polymers have been realized through selective modification of β -CD. However, to date, strictly biphasic Janus nanoparticles have not been realized.^[135] The combination of two dissimilar functional materials is a promising area for discovering novel properties and applications. Recently, the preparation of 1D nanorods were reported by applying the same nanoreactor concept and substituting β -CD with cellulose as a macroinitiator.^[136] Ultimately, even more advanced and useful materials will likely be discovered as the complexity, variety, and dimensionality of nanomaterials are improved.

Acknowledgements

This work was supported by the National Natural Science Foundation of China (grant nos. 51322301, 51622301, 51573046, and 61728403), the Air Force Office of Scientific Research (FA9550-16-1-0187), and the National Science Foundation (CMMI 1562075, CMMI 172313, and DMR 1709420). X.L. gratefully acknowledges financial support from the China Scholarship Council.

Conflict of interest

The authors declare no conflict of interest.

How to cite: *Angew. Chem. Int. Ed.* **2018**, 57, 2046–2070
Angew. Chem. **2018**, 130, 2066–2093

- [1] K. Saha, S. S. Agasti, C. Kim, X. Li, V. M. Rotello, *Chem. Rev.* **2012**, 112, 2739–2779.
- [2] R. Bardhan, S. Lal, A. Joshi, N. J. Halas, *Acc. Chem. Res.* **2011**, 44, 936–946.
- [3] W. Qin, J. Hou, D. A. Bonnell, *Nano Lett.* **2015**, 15, 211–217.
- [4] a) M. Chen, D. W. Goodman, *Acc. Chem. Res.* **2006**, 39, 739–746; b) P. Zhao, N. Li, D. Astruc, *Coord. Chem. Rev.* **2013**, 257, 638–665.
- [5] J. K. Lung, J. C. Huang, D. C. Tien, C. Y. Liao, K. H. Tseng, T. T. Tsung, W. S. Kao, T. H. Tsai, C. S. Jwo, H. M. Lin, *J. Alloys Compd.* **2007**, 434, 655–658.
- [6] D. T. Nguyen, D. J. Kim, K. S. Kim, *Micron* **2011**, 42, 207–227.
- [7] Y. Liang, Y. Li, H. Wang, J. Zhou, J. Wang, T. Regier, H. Dai, *Nat. Mater.* **2011**, 10, 780–786.
- [8] C. Murray, D. J. Norris, M. G. Bawendi, *J. Am. Chem. Soc.* **1993**, 115, 8706–8715.
- [9] P. Yang, D. Zhao, D. I. Margolese, B. F. Chmelka, G. D. Stucky, *Nature* **1998**, 396, 152–155.
- [10] V. Juttukonda, R. L. Paddock, J. E. Raymond, D. Denomme, A. E. Richardson, L. E. Slusher, B. D. Fahlman, *J. Am. Chem. Soc.* **2006**, 128, 420–421.
- [11] X. Pang, L. Zhao, W. Han, X. Xin, Z. Lin, *Nat. Nanotechnol.* **2013**, 8, 426–431.
- [12] S. Kango, S. Kalia, A. Celli, J. Njuguna, Y. Habibi, R. Kumar, *Prog. Polym. Sci.* **2013**, 38, 1232–1261.
- [13] B. Wang, B. Li, B. Zhao, C. Y. Li, *J. Am. Chem. Soc.* **2008**, 130, 11594–11595.
- [14] a) A. Rösler, G. W. M. Vandermeulen, H. A. Klok, *Adv. Drug Delivery Rev.* **2012**, 64, 270–279; b) L. Zhang, A. Eisenberg, *Science* **1995**, 268, 1728; c) M. Moffitt, K. Khougaz, A. Eisenberg, *Acc. Chem. Res.* **1996**, 29, 95–102.
- [15] J. Chai, D. Wang, X. Fan, J. M. Buriak, *Nat. Nanotechnol.* **2007**, 2, 500–506.
- [16] M. S. Bakshi, *Adv. Colloid Interface Sci.* **2014**, 213, 1–20.
- [17] S. Förster, M. Antonietti, *Adv. Mater.* **1998**, 10, 195–217.
- [18] a) R. Hong, N. O. Fischer, T. Emrick, V. M. Rotello, *Chem. Mater.* **2005**, 17, 4617–4621; b) G. H. Woehrle, L. O. Brown, J. E. Hutchison, *J. Am. Chem. Soc.* **2005**, 127, 2172–2183.
- [19] D. Ling, M. J. Hackett, T. Hyeon, *Nano Today* **2014**, 9, 457–477.
- [20] M. Antonietti, E. Wenz, L. Bronstein, M. Seregina, *Adv. Mater.* **1995**, 7, 1000–1005.
- [21] S. Klingelhöfer, W. Heitz, A. Greiner, S. Oestreich, S. Förster, M. Antonietti, *J. Am. Chem. Soc.* **1997**, 119, 10116–10120.
- [22] M. V. Seregina, L. M. Bronstein, O. A. Platonova, D. M. Chernyshov, P. M. Valetsky, J. Hartmann, E. Wenz, M. Antonietti, *Chem. Mater.* **1997**, 9, 923–931.
- [23] C. H. Braun, T. V. Richter, F. Schacher, A. H. Müller, E. J. Crossland, S. Ludwigs, *Macromol. Rapid Commun.* **2010**, 31, 729–734.
- [24] M. Siebert, K. Albrecht, R. Spiertz, H. Keul, M. Möller, *Soft Matter* **2011**, 7, 587–594.
- [25] a) M. Moffitt, H. Vali, A. Eisenberg, *Chem. Mater.* **1998**, 10, 1021–1028; b) H. Zhao, E. P. Douglas, B. S. Harrison, K. S. Schanze, *Langmuir* **2001**, 17, 8428–8433; c) M. Moffitt, L. McMahon, V. Pessel, A. Eisenberg, *Chem. Mater.* **1995**, 7, 1185–1192.
- [26] K. Tarasov, D. Houssein, M. Destarac, N. Marcotte, C. Gérardin, D. Tichit, *New J. Chem.* **2013**, 37, 508–514.
- [27] a) S. R. Ahmed, P. Kofinas, *Macromolecules* **2002**, 35, 3338–3341; b) S. R. Ahmed, S. B. Ogale, G. C. Papaefthymiou, R. Ramesh, P. Kofinas, *Appl. Phys. Lett.* **2002**, 80, 1616–1618.
- [28] a) W. Han, B. Li, Z. Lin, *ACS Nano* **2013**, 7, 6079–6085; b) B. Li, W. Han, B. Jiang, Z. Lin, *ACS Nano* **2014**, 8, 2936–2942; c) B. Li, W. Han, M. Byun, L. Zhu, Q. Zou, Z. Lin, *ACS Nano* **2013**, 7, 4326–4333.
- [29] G. Riess, *Prog. Polym. Sci.* **2003**, 28, 1107–1170.
- [30] G. Kästle, H. G. Boyen, F. Weigl, G. Lengel, T. Herzog, P. Ziemann, S. Riethmüller, O. Mayer, C. Hartmann, J. P. Spatz, *Adv. Funct. Mater.* **2003**, 13, 853–861.
- [31] M. Moffitt, A. Eisenberg, *Macromolecules* **1997**, 30, 4363–4373.
- [32] L. M. Bronstein, S. N. Sidorov, P. M. Valetsky, J. Hartmann, H. Cölfen, M. Antonietti, *Langmuir* **1999**, 15, 6256–6262.

- [33] a) L. M. Bronstein, S. N. Sidorov, A. Y. Gourkova, P. M. Valetsky, J. Hartmann, M. Breulmann, H. Cölfen, M. Antonietti, *Inorg. Chim. Acta* **1998**, 280, 348–354; b) L. Qi, H. Cölfen, M. Antonietti, *Nano Lett.* **2001**, 1, 61–65.
- [34] a) R. S. Underhill, G. Liu, *Chem. Mater.* **2000**, 12, 2082–2091; b) R. S. Underhill, G. Liu, *Chem. Mater.* **2000**, 12, 3633–3641.
- [35] K. O. Sebakhy, S. Kessel, M. J. Monteiro, *Macromolecules* **2010**, 43, 9598–9600.
- [36] W. A. Braunecker, K. Matyjaszewski, *Prog. Polym. Sci.* **2007**, 32, 93–146.
- [37] J. S. Wang, K. Matyjaszewski, *J. Am. Chem. Soc.* **1995**, 117, 5614–5615.
- [38] J. Chiefari, Y. K. Chong, F. Ercole, J. Krstina, J. Jeffery, T. P. T. Le, R. T. A. Mayadunne, G. F. Meijs, C. L. Moad, G. Moad, E. Rizzardo, S. H. Thang, *Macromolecules* **1998**, 31, 5559–5562.
- [39] M. K. Georges, R. P. Veregin, P. M. Kazmaier, G. K. Hamer, *Macromolecules* **1993**, 26, 2987–2988.
- [40] M. Szwarc, *J. Polym. Sci. Part A* **1998**, 36, V–XIII.
- [41] a) T. Pintauer, K. Matyjaszewski, *Chem. Soc. Rev.* **2008**, 37, 1087–1097; b) F. di Lena, K. Matyjaszewski, *Prog. Polym. Sci.* **2010**, 35, 959–1021; c) K. Matyjaszewski, N. V. Tsarevsky, *Nat. Chem.* **2009**, 1, 276–288.
- [42] G. Moad, E. Rizzardo, S. H. Thang, *Polymer* **2008**, 49, 1079–1131.
- [43] Y. Mai, A. Eisenberg, *Chem. Soc. Rev.* **2012**, 41, 5969–5985.
- [44] a) D. M. Vriezema, M. C. Aragonès, J. A. Elemans, J. J. Cornelissen, A. E. Rowan, R. J. Nolte, *Chem. Rev.* **2005**, 105, 1445–1490; b) A. Blanazs, S. P. Armes, A. J. Ryan, *Macromol. Rapid Commun.* **2009**, 30, 267–277.
- [45] H. Cölfen, *Macromol. Rapid Commun.* **2001**, 22, 219–252.
- [46] M. N. Misra, W. L. Mattice, *Macromolecules* **1995**, 28, 1444–1457.
- [47] C. Tsitsilianis, V. Sfika, *Macromol. Rapid Commun.* **2001**, 22, 647–651.
- [48] J. F. Gohy, N. Willet, S. Varshney, J. X. Zhang, R. Jérôme, *Angew. Chem.* **2001**, 113, 3314–3316.
- [49] a) W. Zheng, Z. G. Wang, *Macromolecules* **1995**, 28, 7215–7223; b) A. O. Moughton, M. A. Hillmyer, T. P. Lodge, *Macromolecules* **2012**, 45, 2–19.
- [50] S. N. Sidorov, L. M. Bronstein, Y. A. Kabachii, P. M. Valetsky, P. L. Soo, D. Maysinger, A. Eisenberg, *Langmuir* **2004**, 20, 3543–3550.
- [51] a) N. Duxin, F. Liu, H. Vali, A. Eisenberg, *J. Am. Chem. Soc.* **2005**, 127, 10063–10069; b) H. Yusuf, W. G. Kim, D. H. Lee, Y. Guo, M. G. Moffitt, *Langmuir* **2007**, 23, 868–878.
- [52] O. Platonova, L. Bronstein, S. Solodovnikov, I. Yanovskaya, E. Obolonkova, P. Valetsky, E. Wenz, M. Antonietti, *Colloid Polym. Sci.* **1997**, 275, 426–431.
- [53] M. Möller, J. P. Spatz, A. Roescher, *Adv. Mater.* **1996**, 8, 337–340.
- [54] a) S. Papp, L. Körösi, B. Gool, T. Dederichs, P. Mela, M. Möller, I. Dékány, *J. Therm. Anal. Calorim.* **2010**, 101, 865–872; b) S. Mössmer, J. P. Spatz, M. Möller, T. Aberle, J. Schmidt, W. Burchard, *Macromolecules* **2000**, 33, 4791–4798.
- [55] X. W. D. Lou, L. A. Archer, Z. Yang, *Adv. Mater.* **2008**, 20, 3987–4019.
- [56] B. P. Bastakoti, S. Guragain, Y. Yokoyama, S.-i. Yusa, K. Nakashima, *Langmuir* **2011**, 27, 379–384.
- [57] B. P. Bastakoti, M. Inoue, S. I. Yusa, S. H. Liao, K. C. W. Wu, K. Nakashima, Y. Yamauchi, *Chem. Commun.* **2012**, 48, 6532–6534.
- [58] M. Han, X. Yin, L. Kong, M. Li, W. Duan, L. Zhang, L. Cheng, *J. Mater. Chem. A* **2014**, 2, 16403–16409.
- [59] a) F. Caruso, R. A. Caruso, H. Möhwald, *Science* **1998**, 282, 1111–1114; b) F. Caruso, *Chem. Eur. J.* **2000**, 6, 413–419.
- [60] J. Hu, M. Chen, X. Fang, L. Wu, *Chem. Soc. Rev.* **2011**, 40, 5472–5491.
- [61] A. M. Mydul, H. Kimiko, Y. Chihoro, Y. Shin-ichi, N. Kenichi, *Bull. Chem. Soc. Jpn.* **2015**, 88, 124–126.
- [62] a) D. Zhang, L. Qi, J. Ma, H. Cheng, *Adv. Mater.* **2002**, 14, 1499–1502; b) L. Qi, J. Li, J. Ma, *Adv. Mater.* **2002**, 14, 300–303.
- [63] a) Y. Ma, L. Qi, J. Ma, H. Cheng, *Langmuir* **2003**, 19, 4040–4042; b) C. Nardin, S. Thoeni, J. Widmer, M. Winterhalter, W. Meier, *Chem. Commun.* **2000**, 1433–1434.
- [64] M. Sasidharan, K. Nakashima, *Acc. Chem. Res.* **2014**, 47, 157–167.
- [65] a) A. Khanal, Y. Inoue, M. Yada, K. Nakashima, *J. Am. Chem. Soc.* **2007**, 129, 1534–1535; b) D. Liu, K. Nakashima, *Inorg. Chem.* **2009**, 48, 3898–3900; c) M. Sasidharan, D. Liu, N. Gunawardhana, M. Yoshio, K. Nakashima, *J. Mater. Chem.* **2011**, 21, 13881–13888; d) D. Liu, M. Sasidharan, K. Nakashima, *J. Colloid Interface Sci.* **2011**, 358, 354–359.
- [66] a) B. P. Bastakoti, S. Guragain, Y. Yokoyama, S. I. Yusa, K. Nakashima, *New J. Chem.* **2012**, 36, 125–129; b) M. Sasidharan, H. N. Luitel, N. Gunawardhana, M. Inoue, S. I. Yusa, T. Watari, K. Nakashima, *Mater. Lett.* **2012**, 73, 4–7; c) M. Sasidharan, K. Nakashima, N. Gunawardhana, T. Yokoi, M. Inoue, S. I. Yusa, M. Yoshio, T. Tatsumi, *Chem. Commun.* **2011**, 47, 6921–6923; d) M. Sasidharan, N. Gunawardhana, H. N. Luitel, T. Yokoi, M. Inoue, S. I. Yusa, T. Watari, M. Yoshio, T. Tatsumi, K. Nakashima, *J. Colloid Interface Sci.* **2012**, 370, 51–57; e) Z. Shuo, Y. Shin-ichi, N. Kenichi, *Bull. Chem. Soc. Jpn.* **2013**, 86, 884–890; f) A. M. Mydul, Z. Wenwen, Z. Shuo, Y. Shin-ichi, N. Hideyuki, N. Kenichi, *Chem. Lett.* **2014**, 43, 1426–1428.
- [67] N. M. Dang, W. W. Zhao, S. I. Yusa, H. Noguchi, K. Nakashima, *New J. Chem.* **2015**, 39, 4726–4730.
- [68] a) J. Liu, D. Liu, Y. Yokoyama, S. I. Yusa, K. Nakashima, *Langmuir* **2009**, 25, 739–743; b) J. Liu, M. Sasidharan, D. Liu, Y. Yokoyama, S. I. Yusa, K. Nakashima, *Mater. Lett.* **2012**, 66, 25–28.
- [69] J. F. Gohy, N. Willet, S. K. Varshney, J. X. Zhang, R. Jérôme, *e-Polymers* **2002**, 2, 517–526.
- [70] R. G. Chaudhuri, S. Paria, *Chem. Rev.* **2012**, 112, 2373–2433.
- [71] a) H. Sakai, T. Kanda, H. Shibata, T. Ohkubo, M. Abe, *J. Am. Chem. Soc.* **2006**, 128, 4944–4945; b) L. Jing, C. Yang, R. Qiao, M. Niu, M. Du, D. Wang, M. Gao, *Chem. Mater.* **2010**, 22, 420–427; c) P. Yang, M. Ando, N. Murase, *Langmuir* **2011**, 27, 9535–9540.
- [72] a) L. M. Liz-Marzán, M. Giersig, P. Mulvaney, *Langmuir* **1996**, 12, 4329–4335; b) T. Ung, L. M. Liz-Marzán, P. Mulvaney, *J. Phys. Chem. B* **2001**, 105, 3441–3452.
- [73] a) Y. Lu, B. He, J. Shen, J. Li, W. Yang, M. Yin, *Nanoscale* **2015**, 7, 1606–1609; b) J. Shen, G. Chen, T. Y. Ohulchanskyy, S. J. Kesseli, S. Buchholz, Z. Li, P. N. Prasad, G. Han, *Small* **2013**, 9, 3213–3217.
- [74] M. Casavola, R. Buonsanti, G. Caputo, P. D. Cozzoli, *Eur. J. Inorg. Chem.* **2008**, 837–854.
- [75] B. P. Bastakoti, S. Guragain, S. I. Yusa, K. Nakashima, *RSC Adv.* **2012**, 2, 5938.
- [76] E. Seo, S. J. Ko, S. H. Min, J. Y. Kim, B. S. Kim, *Chem. Mater.* **2015**, 27, 4789–4798.
- [77] M. Aizawa, J. M. Buriak, *J. Am. Chem. Soc.* **2006**, 128, 5877–5886.
- [78] S. M. Jeon, K. Y. Jang, S. H. Lee, H. W. Park, B. H. Sohn, *Langmuir* **2008**, 24, 11137–11140.
- [79] H. D. Koh, S. Park, T. P. Russell, *ACS Nano* **2010**, 4, 1124–1130.
- [80] J. Simms, *Rubber Chem. Technol.* **1991**, 64, 139–151.
- [81] L. J. Fetters, A. D. Kiss, D. S. Pearson, G. F. Quack, F. J. Vitus, *Macromolecules* **1993**, 26, 647–654.
- [82] H. Gao, K. Matyjaszewski, *Macromolecules* **2006**, 39, 3154–3160.

- [83] K. Min, H. Gao, K. Matyjaszewski, *J. Am. Chem. Soc.* **2005**, *127*, 3825–3830.
- [84] X. Hao, C. Nilsson, M. Jesberger, M. H. Stenzel, E. Malmström, T. P. Davis, E. Östmark, C. Barner-Kowollik, *J. Polym. Sci. Part A* **2004**, *42*, 5877–5890.
- [85] M. Jesberger, L. Barner, M. H. Stenzel, E. Malmström, T. P. Davis, C. Barner-Kowollik, *J. Polym. Sci. Part A* **2003**, *41*, 3847–3861.
- [86] M. H. Stenzel-Rosenbaum, T. P. Davis, V. Chen, A. G. Fane, *Macromolecules* **2001**, *34*, 5433–5438.
- [87] J. M. Ren, T. G. McKenzie, Q. Fu, E. H. Wong, J. Xu, Z. An, S. Shanmugam, T. P. Davis, C. Boyer, G. G. Qiao, *Chem. Rev.* **2016**, *116*, 6743–6836.
- [88] K. Ohno, B. Wong, D. M. Haddleton, *J. Polym. Sci. Part A* **2001**, *39*, 2206–2214.
- [89] a) J. Li, H. Xiao, Y. S. Kim, T. L. Lowe, *J. Polym. Sci. Part A* **2005**, *43*, 6345–6354; b) J. Li, H. Xiao, *Tetrahedron Lett.* **2005**, *46*, 2227–2229.
- [90] B. Jiang, X. Pang, B. Li, Z. Lin, *J. Am. Chem. Soc.* **2015**, *137*, 11760–11767.
- [91] H. Xu, X. Pang, Y. He, M. He, J. Jung, H. Xia, Z. Lin, *Angew. Chem. Int. Ed.* **2015**, *54*, 4636–4640; *Angew. Chem.* **2015**, *127*, 4719–4723.
- [92] a) F. A. Plamper, H. Becker, M. Lanzendörfer, M. Patel, A. Wittemann, M. Ballauff, A. H. E. Müller, *Macromol. Chem. Phys.* **2005**, *206*, 1813–1825; b) K. Karaky, S. Reynaud, L. Billon, J. François, Y. Chreim, *J. Polym. Sci. Part A* **2005**, *43*, 5186–5194.
- [93] C. Feng, X. Pang, Y. He, Y. Chen, G. Zhang, Z. Lin, *Polym. Chem.* **2015**, *6*, 5190–5197.
- [94] H. C. Kolb, M. Finn, K. B. Sharpless, *Angew. Chem. Int. Ed.* **2001**, *40*, 2004–2021; *Angew. Chem.* **2001**, *113*, 2056–2075.
- [95] J. Xu, S. Liu, *J. Polym. Sci. Part A* **2009**, *47*, 404–419.
- [96] X. Pang, L. Zhao, C. Feng, Z. Lin, *Macromolecules* **2011**, *44*, 7176–7183.
- [97] X. Pang, L. Zhao, M. Akinc, J. K. Kim, Z. Lin, *Macromolecules* **2011**, *44*, 3746–3752.
- [98] Y. Chen, Y. J. Yoon, X. Pang, Y. He, J. Jung, C. Feng, G. Zhang, Z. Lin, *Small* **2016**, *12*, 6714–6723.
- [99] D. Yang, X. Pang, Y. He, Y. Wang, G. Chen, W. Wang, Z. Lin, *Angew. Chem. Int. Ed.* **2015**, *54*, 12091–12096; *Angew. Chem.* **2015**, *127*, 12259–12264.
- [100] a) X. Zhang, W. Lin, L. Wen, N. Yao, S. Nie, L. Zhang, *Phys. Chem. Chem. Phys.* **2016**, *18*, 26519–26529; b) N. Yao, W. Lin, X. Zhang, H. Gu, L. Zhang, *J. Polym. Sci. Part A* **2016**, *54*, 186–196.
- [101] A. Harada, J. Li, M. Kamachi, *Nature* **1992**, *356*, 325.
- [102] H. Xu, Y. Xu, X. Pang, Y. He, J. Jung, H. Xia, Z. Lin, *Sci. Adv.* **2015**, *1*, e1500025.
- [103] S. E. Skrabalak, J. Chen, Y. Sun, X. Lu, L. Au, C. M. Cobley, Y. Xia, *Acc. Chem. Res.* **2008**, *41*, 1587–1595.
- [104] E. Prodan, C. Radloff, N. J. Halas, P. Nordlander, *Science* **2003**, *302*, 419–422.
- [105] S. J. Oldenburg, S. L. Westcott, R. D. Averitt, N. J. Halas, *J. Chem. Phys.* **1999**, *111*, 4729–4735.
- [106] H. P. Liang, L. J. Wan, C. L. Bai, L. Jiang, *J. Phys. Chem. B* **2005**, *109*, 7795–7800.
- [107] J. Zhang, Y. Tang, K. Lee, M. Ouyang, *Science* **2010**, *327*, 1634–1638.
- [108] A. Roldan, D. Santos-Carballal, N. H. de Leeuw, *J. Chem. Phys.* **2013**, *138*, 204712.
- [109] M. Wang, X. Pang, D. Zheng, Y. He, L. Sun, C. Lin, Z. Lin, *J. Mater. Chem. A* **2016**, *4*, 7190–7199.
- [110] X. Xin, G. Xu, Z. Zhang, Y. Chen, F. Wang, *Eur. Polym. J.* **2007**, *43*, 3106–3111.
- [111] C. Rao, G. Kulkarni, P. J. Thomas, P. P. Edwards, *Chem. Eur. J.* **2002**, *8*, 28–35.
- [112] M. Hu, J. Chen, Z.-Y. Li, L. Au, G. V. Hartland, X. Li, M. Marquez, Y. Xia, *Chem. Soc. Rev.* **2006**, *35*, 1084–1094.
- [113] S. Linic, P. Christopher, D. B. Ingram, *Nat. Mater.* **2011**, *10*, 911–921.
- [114] S. Logunov, T. Ahmadi, M. El-Sayed, J. Khoury, R. Whetten, *J. Phys. Chem. B* **1997**, *101*, 3713–3719.
- [115] a) M. Zaitoun, W. R. Mason, C. Lin, *J. Phys. Chem. B* **2001**, *105*, 6780–6784; b) J. S. Melinger, V. D. Kleiman, D. McMorrow, F. Gröhn, B. J. Bauer, E. Amis, *J. Phys. Chem. A* **2003**, *107*, 3424–3431.
- [116] Z. Xu, Y. Hou, S. Sun, *J. Am. Chem. Soc.* **2007**, *129*, 8698–8699.
- [117] X. Zhang, Y. L. Chen, R.-S. Liu, D. P. Tsai, *Rep. Prog. Phys.* **2013**, *76*, 046401.
- [118] S. Xuan, Y. X. J. Wang, J. C. Yu, K. C.-F. Leung, *Chem. Mater.* **2009**, *21*, 5079–5087.
- [119] X. Wang, N. You, F. Lan, P. Fu, Z. Cui, X. Pang, M. Liu, Q. Zhao, *RSC Adv.* **2017**, *7*, 7789–7792.
- [120] M. Z. Rong, M. Q. Zhang, Y. X. Zheng, H. M. Zeng, R. Walter, K. Friedrich, *Polymer* **2001**, *42*, 167–183.
- [121] C. Ahn, K. Rabe, J.-M. Triscone, *Science* **2004**, *303*, 488–491.
- [122] Z. Zhao, V. Buscaglia, M. Viviani, M. T. Buscaglia, L. Mitoseriu, A. Testino, M. Nygren, M. Johnsson, P. Nanni, *Phys. Rev. B* **2004**, *70*, 024107.
- [123] X. Pang, Y. He, B. Jiang, J. Iocozzia, L. Zhao, H. Guo, J. Liu, M. Akinc, N. Bowler, X. Tan, Z. Lin, *Nanoscale* **2013**, *5*, 8695–8702.
- [124] a) G. A. Somorjai, J. Y. Park, *Angew. Chem. Int. Ed.* **2008**, *47*, 9212–9228; *Angew. Chem.* **2008**, *120*, 9352–9368; b) F. Zaera, *Catal. Lett.* **2012**, *142*, 501–516.
- [125] C. H. Bartholomew, *Appl. Catal. A* **2001**, *212*, 17–60.
- [126] E. Seo, J. Kim, Y. Hong, Y. S. Kim, D. Lee, B.-S. Kim, *J. Phys. Chem. C* **2013**, *117*, 11686–11693.
- [127] a) M. Zhao, R. M. Crooks, *Angew. Chem. Int. Ed.* **1999**, *38*, 364–365; *Angew. Chem.* **1999**, *111*, 375–377; b) L. K. Yeung, R. M. Crooks, *Nano Lett.* **2001**, *1*, 14–17.
- [128] Q. Zhang, I. Lee, J. B. Joo, F. Zaera, Y. Yin, *Acc. Chem. Res.* **2012**, *46*, 1816–1824.
- [129] V. Subramanian, E. E. Wolf, P. V. Kamat, *J. Am. Chem. Soc.* **2004**, *126*, 4943–4950.
- [130] M. He, X. Pang, X. Liu, B. Jiang, Y. He, H. Snaith, Z. Lin, *Angew. Chem. Int. Ed.* **2016**, *55*, 4280–4284; *Angew. Chem.* **2016**, *128*, 4352–4356.
- [131] D. Zheng, X. Pang, M. Wang, Y. He, C. Lin, Z. Lin, *Chem. Mater.* **2015**, *27*, 5271–5278.
- [132] B. Jiang, C. Han, B. Li, Y. He, Z. Lin, *ACS Nano* **2016**, *10*, 2728–2735.
- [133] S. Zhao, Z. Wang, Y. He, B. Jiang, Y. Harn, X. Liu, F. Yu, F. Feng, Q. Shen, Z. Lin, *ACS Energy Lett.* **2017**, *2*, 111–116.
- [134] M. Sasidharan, K. Nakashima, N. Gunawardhana, T. Yokoi, M. Ito, M. Inoue, S.-i. Yusa, M. Yoshio, T. Tatsumi, *Nanoscale* **2011**, *3*, 4768–4773.
- [135] X. Pang, C. Wan, M. Wang, Z. Lin, *Angew. Chem. Int. Ed.* **2014**, *53*, 5524–5538; *Angew. Chem.* **2014**, *126*, 5630–5644.
- [136] X. Pang, Y. He, J. Jung, Z. Lin, *Science* **2016**, *353*, 1268–1272.

Manuscript received: May 16, 2017

Revised manuscript received: August 3, 2017

Accepted manuscript online: August 7, 2017

Version of record online: January 15, 2018